CENP-E initiates chromosome congression by opposing Aurora kinases to promote end-on attachments

Kruno Vukušić*, Iva M. Tolić*

Division of Molecular Biology, Ruđer Bošković Institute, Zagreb, Croatia

*Corresponding authors

E-mail: kvukusic@irb.hr, tolic@irb.hr

ABSTRACT

Chromosome congression to the spindle equator is crucial for accurate cell division. The kinetochore motor protein CENP-E/kinesin-7 is uniquely required for the rapid congression of chromosomes near centrosomes. Current models suggest that CENP-E drives congression by gliding kinetochores along microtubules independently of chromosome biorientation. Here, by studying chromosome movement under different levels of CENP-E activity, we propose an alternative model in which CENP-E initiates congression by promoting the formation or stabilization of end-on attachments at kinetochores, rather than by directly propelling the chromosomes. CENP-E accelerates congression initiation by opposing Aurora kinase activity, but subsequent chromosome movement toward the equator does not depend on CENP-E. Without CENP-E, stabilization of end-on attachments is delayed due to Aurora kinase-mediated phosphorylation of microtubule-binding proteins on kinetochores and the expansion of the fibrous corona. We propose that CENP-E counters this inhibition by reducing Aurora B-mediated phosphorylation of outer kinetochore proteins in a BubR1-dependent manner, thereby stabilizing end-on attachments, facilitating the removal of the fibrous corona, and initiating biorientation-dependent chromosome movement.

Keywords: Mitosis/Chromosome congression/Kinetochore/Aurora kinases/CENP-E

INTRODUCTION

To ensure equal segregation into the two daughter cells, duplicated chromosomes achieve biorientation by attaching to microtubules extending from opposite spindle poles, thereby satisfying the spindle assembly checkpoint (SAC) (Maiato et al., 2017; McAinsh and Kops, 2023; Valdez et al., 2023). During early mitosis, chromosomes move towards the equatorial region of the spindle in a process known as chromosome congression (Barisic et al., 2014). Chromosomes positioned at the center of the nucleus at the onset of mitosis rapidly achieve biorientation and are characterized by shorter congression movements, without requiring kinetochore molecular motors (Itoh et al., 2018; Barisic et al., 2014). In contrast, chromosomes positioned near the spindle poles, referred to as polar chromosomes, require the activity of the kinetochore motor protein CENtromere-associated Protein-E (CENP-E/kinesin-7) for more prominent congression movements (Barisic et al., 2014). Recent studies identified that polar chromosomes are particularly prone to alignment failure during shortened mitosis in healthy cells and unperturbed mitosis in cancer cells (Gomes et al., 2022; Tucker et al., 2023; Klaasen et al., 2022). Thus, the congression of polar chromosomes seems to exhibit distinct dynamics, regulatory mechanisms, and final efficiency (Vukušić and Tolić, 2022).

CENP-E function in chromosome movement has been studied extensively (Yen et al., 1992, 1991; Weaver et al., 2003; Schaar et al., 1997; Mao et al., 2005; Kapoor et al., 2006; Kim et al., 2008; Gudimchuk et al., 2013; Yao et al., 1997; Shrestha and Draviam, 2013; Bancroft et al., 2015; Barisic et al., 2014; Maiato et al., 2017; Auckland and McAinsh, 2015). The prevailing model posits that CENP-E drives the gliding of polar kinetochores, which are laterally attached to microtubules, toward the equatorial plate through its microtubule plus-end directed motor activity (Kapoor et al., 2000; Cai et al., 2009; Walczak et al., 2010; Yu et al., 2019). This model suggests that chromosome congression is decoupled from chromosome biorientation, which occurs near the metaphase plate (Kapoor et al., 2006; Cai et al., 2009). The preference for which motor drives kinetochore movement in the tug-of-war between plus-end directed CENP-E and minus-end directed dynein is influenced by several factors. This includes a single-site phosphorylation of CENP-E at T422 by Aurora kinases near the spindle poles (Kim et al., 2010) and the increased detyrosination of tubulin on kinetochore fibers (Barisic et al., 2015). Both modifications enhance the motor activity of CENP-E (Barisic and Maiato, 2015; Kops and Gassmann, 2020). CENP-E is recruited to an unattached outer kinetochore by BuBR1 (Cmentowski et al., 2023), and to a fibrous corona, which sheds from the kinetochore upon stable end-on attachment formation (Cooke et al., 1997; Yen et al., 1991; Kops and Gassmann, 2020), by the Rod-Zw10-Zwilch (RZZ) and Dynein-Dynactin complexes (Weber et al., 2024; Cmentowski et al., 2023).

Despite the established requirement of CENP-E for chromosome congression, several observations cannot be explained by the current model. First, polar chromosomes initially move toward the spindle center even without CENP-E activity, but they fail to align properly, drifting toward the closer spindle pole (Renda et al., 2022), which contradicts the gliding model of CENP-E function. Second, congression still occurs, albeit with delays, in the complete absence of CENP-E (Kim et al., 2010; Maia et al., 2010; Barisic et al., 2014; Bancroft et al., 2015; Iemura and Tanaka, 2015). However, the extent of similarity between CENP-E-driven congression and

congression occurring independently of CENP-E remains unknown. Consequently, the underlying mechanisms of chromosome congression are still unclear.

Here, we reveal that chromosome congression involves two distinct mechanical steps—initiation and movement. CENP-E is crucial only for initiating congression by facilitating the formation of end-on attachments, rather than directly driving chromosome movement to the spindle equator, which occurs with the same dynamics regardless of CENP-E presence or activity. We arrived at this conclusion by employing a large-scale live-cell imaging strategy using lattice light-sheet microscopy (LLSM). This technique enabled us to simultaneously observe and track numerous chromosome congression events across many cells over time and space. By combining this strategy with reversible chemical inhibition experiments targeting key molecules implicated in congression, we delineated the hierarchical molecular networks underlying this process. Our data demonstrate that CENP-E initiates the stabilization of end-on attachments—a critical initial step in congression—preceding chromosome movement. This is marked by a gradual decrease in SAC proteins and the concurrent formation of end-on attachments observed via super-resolution microscopy. Aurora kinases counter congression initiation by destabilizing end-on attachments. CENP-E counteracts the activity of Aurora kinases in a BubR1-dependent manner, promoting rapid formation of end-on attachments and subsequent chromosome congression movement. Additionally, we found that in the absence of CENP-E, the expansion of the fibrous corona, which depends on Aurora B kinase activity, also impedes the formation of end-on attachments and chromosome congression. In summary, we demonstrate that chromosome biorientation is coupled with chromosome congression near the spindle poles, with CENP-E serving as a crucial link between the two processes and Aurora kinases acting as the key regulatory elements.

RESULTS

CENP-E is essential only for the initiation of movement during chromosome congression

To unravel the complex molecular pathways involved in chromosome congression with respect to CENP-E activity (Maiato et al., 2017), we developed an assay to systematically investigate the interplay between CENP-E and other molecular players implicated in this process. By usage of CENP-E inactivation or depletion, referred to jointly as CENP-E perturbation, we created two distinct populations of chromosomes—those aligned at the spindle midplane and polar chromosomes—resulting in mitotic spindles with synchronized chromosomes near the spindle poles (Fig. 1A; and Fig. S1). This approach minimizes the variabilities between chromosomes typically observed in unperturbed mitosis (Magidson et al., 2011). To simultaneously image many individual cells (1.5 mm field of view) in complete volumes (35 μm depth) with high spatiotemporal resolution (~350 nm and 2 min/image) for a prolonged duration (>24 hours) and with minimal phototoxicity, we established a live-cell imaging approach based on lattice light-sheet microscopy (Fig. 1A; and Video 1, see also Fig. S1 for comparison with confocal microscopy). We combined this large-scale imaging approach with an experimental design that allowed us to acutely vary the activity or presence of CENP-E in the human non-transformed cell line RPE-1. This approach created conditions with varying CENP-E activity: (1) 'CENP-E reactivated,' achieved by acute reactivation of CENP-E motor activity via washout following inhibition with the small-molecule inhibitor GSK923295 (Wood et al., 2010); (2) 'CENP-E depleted,' achieved by using small interfering RNAs (siRNAs) to deplete CENP-E; (3) 'CENP-E inhibited,' achieved by continuous inhibition of CENP-E with GSK923295; and (4) 'control,' treated with DMSO (Fig. 1B). We then tracked the 3D positions of centrosomes and kinetochores over time in randomly selected cells (see Methods). The depletion effectiveness for all targets throughout the manuscript is provided in Fig. S2A-G.

We reasoned that if chromosome congression is driven by CENP-E, the movement of polar chromosomes towards metaphase plate would differ in the presence or absence of CENP-E activity. Conversely, if CENP-E is involved in other processes essential for congression but not directly responsible for movement, the movement of polar chromosomes would be similar regardless of CENP-E activity (Fig. 1C). Following reactivation of CENP-E, all polar chromosomes successfully congressed to the metaphase plate during 60 min (Fig. 1D; and Fig. S1A; and Video 2). Polar kinetochores approached the equatorial region in a highly uniform manner, characterized by an initial slower and a faster second phase of movement (Fig. 1D; and Fig. S1A) (Kapoor et al., 2006), a gradual increase in interkinetochore distance (Fig. S1B), and a gradual reorientation of the axis between sister kinetochores toward the main spindle axis (Fig. S1C). This dynamics is similar to polar kinetochores during early prometaphase in control cells (Fig. 1D; and Fig. S1A-C; and Video 2) (Magidson et al., 2011), although the slow phase of congression was brief or absent in control cells (Fig. 1D). We thus conclude that the CENP-E-driven congression of polar chromosomes after CENP-E reactivation recapitulates the main features of their congression during prometaphase.

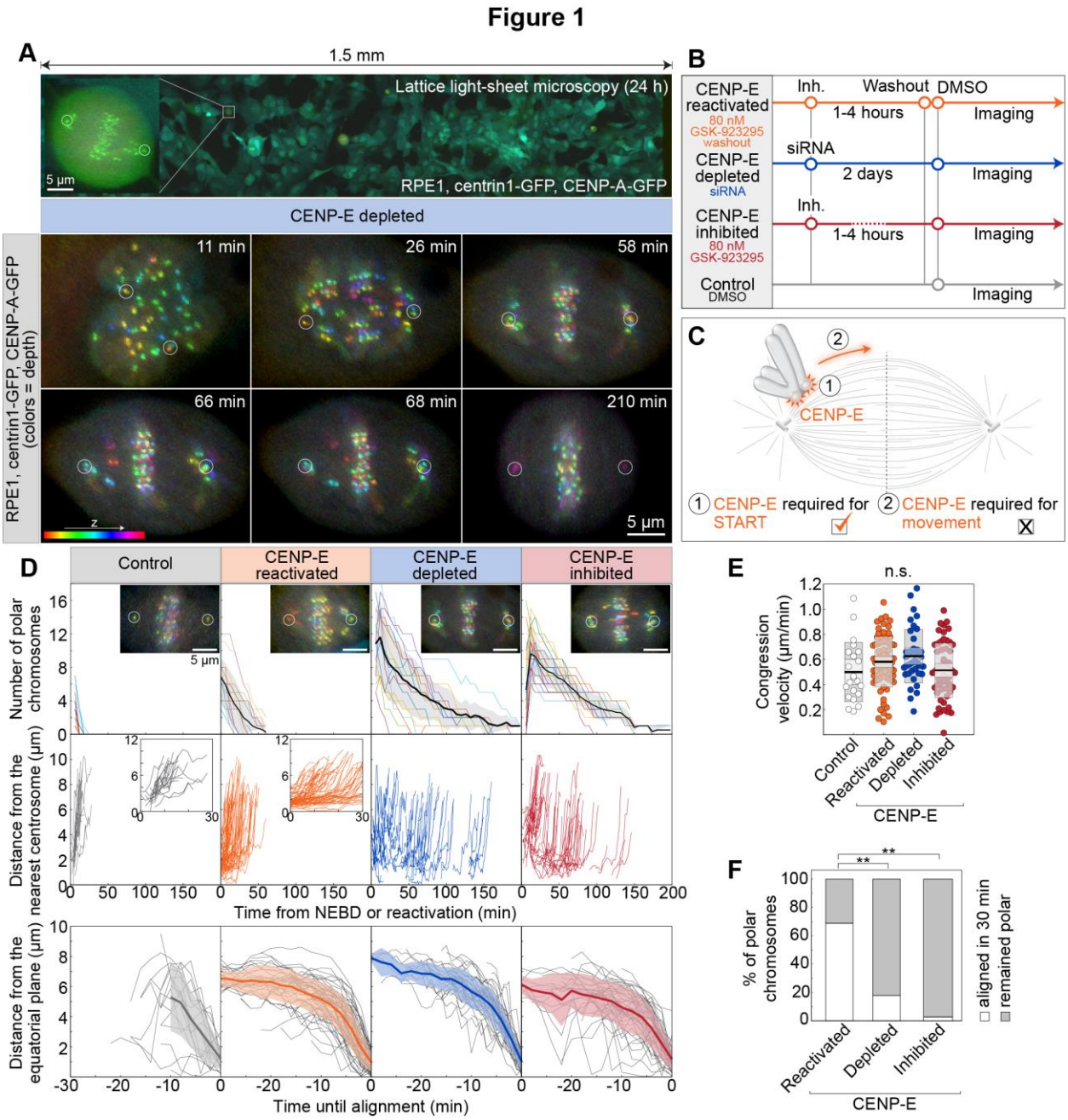

Figure 1. CENP-E activity is required only for the rapid initiation of congression, but not for the subsequent movement of polar chromosomes. (A) The field of imaging is 1.5 mm wide and includes dozens of RPE-1 cells expressing centrin1-GFP (with centrioles encircled in white) and CENPA-GFP, imaged by lattice light sheet microscopy (LLSM). Cells were treated with the 80 nM CENP-E inhibitor GSK-923295 for 3 h prior to imaging. The boxed area on the left showcases a zoom in on one of the mitotic cells from the imaged area, with a scale bar of 5 µm (top). Example of a representative RPE-1 cell undergoing mitosis after CENP-E depletion imaged using the same assay (bottom). The images are maximum projections color coded for depth (see color bar). Time 0 represents the onset of mitosis. (B) Scheme of the protocol to obtain varying and acutely controllable levels of CENP-E activity in cells. (C) Scheme depicting the hypothesis that CENP-

E, depicted by red glow signs, is required for the initiation of chromosome congression (START), depicted by 1, or for the movement of chromosomes during congression, depicted by 2. The tick represents the interpretation favored by the obtained results. (D) Number of polar chromosomes over time under different treatments, depicted in different colors, with representative mitotic cells with centrioles encircled in white in the top right corner (top). Distance from the nearest pole of polar kinetochore pairs in time from nuclear envelope breakdown (NEBD) or washout time for CENP-E reactivated condition, with enlargements of data over the x-axis in the upper right part. The lines represent all kinetochores that were defined as polar 10 minutes after nuclear envelope breakdown and that we were able to discriminate from neighboring kinetochores immediately prior and during congression movement (middle). Distance from the equatorial plane of kinetochore pairs over time until alignment in different treatments. Thick lines represent means, and the grey areas over means represent standard deviations (bottom). (E) Velocity of chromosome congression during the 6-minute period that precedes alignment for depicted treatments. The black line shows the mean; the light grey and dark grey areas mark the 95% confidence interval on the mean and standard deviation, respectively. Numbers D and E: control (15 cells, 32 kinetochore pairs), reactivated (18 cells, 86 kinetochore pairs), CENP-E depleted (18 cells, 69 kinetochore pairs), inhibited (12 cells, 65 kinetochore pairs), each from at least three independent biological replicates. (F) Percentage of polar kinetochore pairs that aligned (white) or remained polar (grey) during the 30-minute period from the end of prometaphase spindle elongation in the indicated treatments. Numbers F: reactivated (23 cells), depleted (38 cells), inhibited (14 cells), each from at least three independent biological replicates. Statistics: Tukey's HSD test. Symbols indicate: n.s. $P > 0.05$, $^{**}P \leq 0.01$. Inh., inhibited; siRNA, small interfering RNA; NEBD, nuclear envelope breakdown.

How do the dynamics of chromosome congression compare between cells with the active and perturbed CENP-E? In CENP-E depleted and CENP-E inhibited conditions, the number of polar chromosomes decayed gradually during mitosis as chromosomes congressed to the metaphase plate (Fig 1D; and Video 3), resulting in successful congression of majority of polar chromosomes within 3 hours, similar to previous observations (Tovini and McClelland, 2019; Maia et al., 2010; Barisic et al., 2014; Kim et al., 2010). Intriguingly, although polar chromosomes began moving asynchronously during prolonged mitosis (Fig. 1D), their movement toward the plate was highly similar under both active and perturbed CENP-E conditions (Fig. 1D; Fig. S1D; Video 3). This movement was accompanied by an increase in interkinetochore distance and reorientation of the kinetochore pair toward the spindle axis in all conditions (Fig. 1D; Fig. S1A-D). Importantly, the mean velocities of sister kinetochore movement during the 6 minutes prior to joining the plate, which corresponds to the major portion of the congression movement (Fig. 1D; Fig. S1A-D), were indistinguishable across conditions irrespectively of CENP-E activity (Fig. 1E). This suggests that polar chromosomes move from the spindle poles to the equator in a manner independent of CENP-E activity, challenging models in which CENP-E actively transports polar chromosomes to the metaphase plate by gliding them along spindle microtubules.

Since we observed that congression movement remains highly similar regardless of CENP-E presence or activity, our next objective was to understand why the absence of CENP-E leads to

extensive delays in chromosome congression. We found that approximately 20% of polar kinetochores initiated congression movement within 30 minutes following prometaphase spindle elongation under CENP-E perturbed conditions. In contrast, over 85% of polar chromosomes initiated congression when CENP-E was reactivated, and 100% did so under control conditions during the same period (Fig. 1F; Fig. S1A-D; Videos 2 and 3). This suggests that CENP-E plays a role in the initiation of kinetochore movement. Finally, we tested whether the dynamics of congression change with the time spent in mitosis. There was no correlation between the velocity of congression and the time elapsed from the onset of mitosis to the initiation of congression across conditions (Fig. S1E), indicating that the dynamics of chromosome movement during congression are robust to the time a cell spent in mitosis. In conclusion, our findings suggest that while CENP-E does not drive the movement of polar chromosomes to the metaphase plate, it is crucial for the rapid and synchronous initiation of this movement.

The speed of chromosome congression is determined by the rate at which end-on attachments are formed

Having identified that chromosome congression consists of distinct initiation and movement phases, we hypothesized that the initiation phase requires the formation of end-on attachments at polar kinetochores. This led us to propose that CENP-E plays an active role in establishing end-on microtubule attachments at polar kinetochores. To test this hypothesis, we reactivated CENP-E in cells expressing the SAC protein Mad2, which accumulates on kinetochores lacking end-on attachments (Chen et al., 1996; Collin et al., 2013; Kuhn and Dumont, 2017), and tracked the response of kinetochore microtubule attachments to CENP-E reactivation over time. Immediately after CENP-E reactivation, polar kinetochores had high levels of Mad2, indicating the absence of end-on attachments (Fig. 2A and B; and Fig. S3A and B) (Barisic et al., 2014). As a response to CENP-E reactivation, Mad2 levels on polar kinetochores gradually decreased over time (Fig. 2A and B; and Fig. S3A and B, and Video 4), in contrast to the cells in which CENP-E was continuously inhibited and Mad2 levels remained constant (Fig. 2C). Interestingly, the drop of Mad2 on polar kinetochores started, on average, prior to their fast movement towards the equatorial plane although it continued to drop as kinetochores congressed (Fig. 2D; and Fig. S3A-C). In line with that, Mad2 dropped also on kinetochores that did not initiate movement during the imaging, though at a slower rate (Fig. S3B). These results suggest that the formation of end-on attachments at polar kinetochores depends on CENP-E activity and occurs during the initial phase of congression, prior to the rapid movement of the kinetochore toward the metaphase plate.

Figure 2

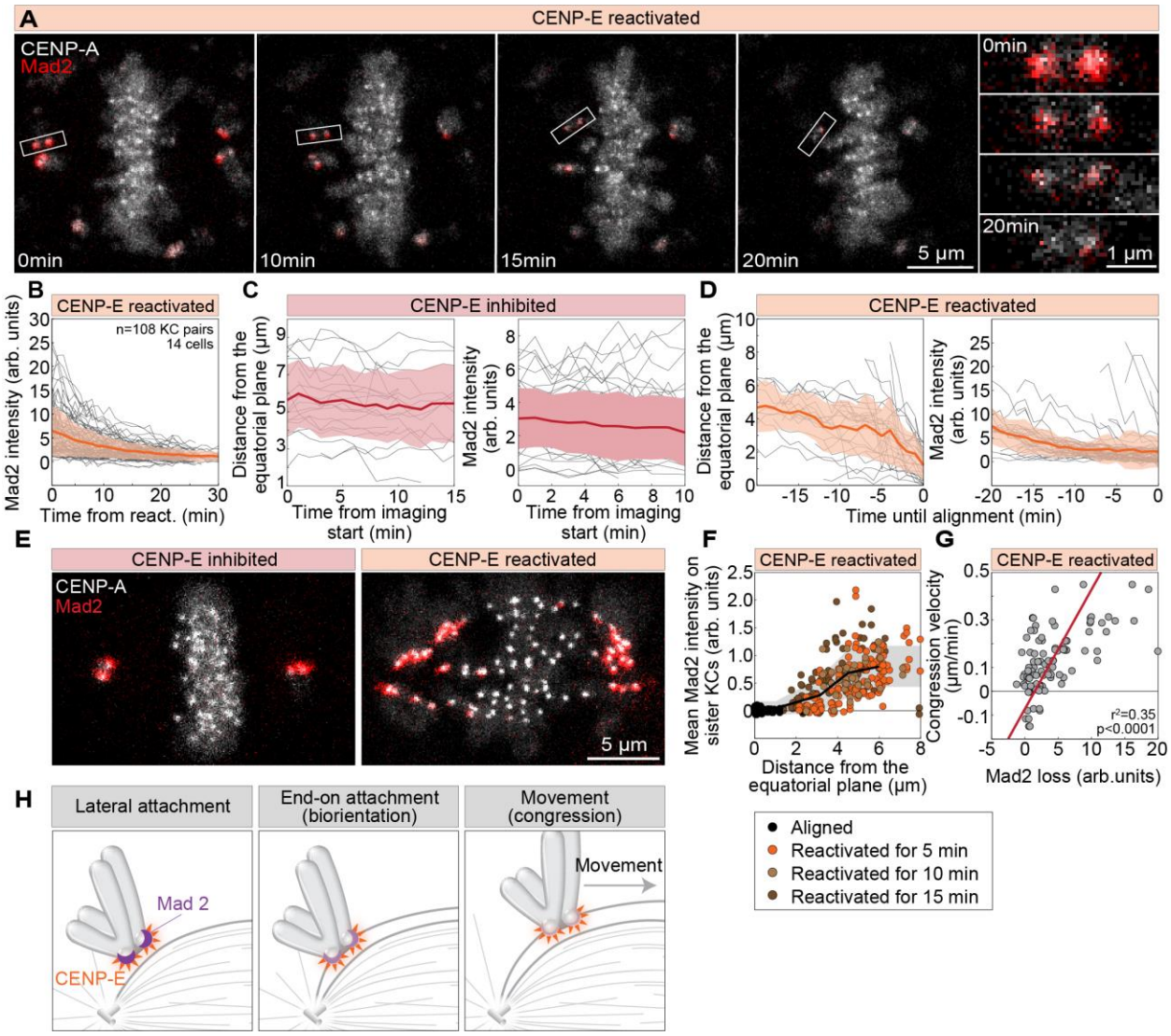

Figure 2. Reactivation of CENP-E is accompanied by the gradual loss of Mad2 from kinetochores, which starts prior to chromosome movement. (A) Representative example of a cell expressing Mad2-mRuby (red) and CENPA-mCerulean (grey) at different times after the washout of the CENP-E inhibitor as depicted. Images on the right are enlargements of sister kinetochores during congression, as per the boxed area on the left. Time 0 represents the washout of the CENP-E inhibitor. (B) Mean Mad2 signal intensity of initially polar sister kinetochore pairs over time from the washout of the CENP-E inhibitor. The thick black line represents the mean, and the orange area around the mean represents the standard deviation. (C) Distance of polar kinetochore pairs from the equatorial plane (left) and mean Mad2 signal intensity (right) of polar sister kinetochore pairs over time in the presence of the CENP-E inhibitor. (D) Distance of polar kinetochore from the equatorial plane (left), and mean Mad2 intensity on polar kinetochore pairs (right) in time until alignment. (E) Representative examples of cells expressing Mad2-mRuby (red) and CENPA-mCerulean (grey) fixed in the presence of CENP-E inhibitor (left) or 5 minutes after the washout of the inhibitor (right). (F) Distance of polar kinetochore pairs from the metaphase

plate over the mean Mad2 signal intensity of kinetochore pairs under indicated conditions. Thick line represents the mean for binned data values, and the grey area over the mean represents the standard deviation of the mean for binned data. (G) Congression velocity during the 30-minute period after CENP-E inhibitor washout over the loss of Mad2 signal intensity in kinetochore pairs and linear regression (line). Negative values represent the movement of the kinetochore pair from the metaphase plate. (H) The diagrams illustrate the loss of Mad2, shown as a purple crescent on the kinetochore, from polar kinetochores prior to the fast movement of the chromosome. CENP-E is depicted in orange at the kinetochore. Note that Mad2 is not completely lost from the kinetochore during congression initiation as complete loss occurs gradually during the congression movement. All images are a maximum projection of all acquired z planes. Numbers not indicated elsewhere: 14 cells, 54 kinetochore pairs (D, and G), 10 cells, 28 kinetochore pairs (B), 26 cells, 135 kinetochore pairs (F), each from at least three independent biological replicates. arb., arbitrary; inh., inhibited; depl, depleted; reac., reactivated; KC, kinetochore.

If end-on conversion is coupled to congression than congressing chromosomes would predominantly come to the equatorial plate already bioriented. Indeed, the average Mad2 signal on sister kinetochores after CENP-E reactivation was higher at the kinetochore pairs that were closer to the spindle pole, and the majority of kinetochores approached the metaphase plate with Mad2 signal intensities indistinguishable from those of aligned kinetochores (Fig. 2E and F). The Mad2 signal was negatively correlated with the distance between sister kinetochores, which serves as a readout of inter-kinetochore tension (Fig. S3D). These results suggest that after CENP-E is reactivated, polar kinetochores progressively establish more end-on attachments with microtubules, generating increased tension on the kinetochores (Kuhn and Dumont, 2017). If the extent of end-on conversion is dictating dynamics of congression, then the average congression speed over a longer period, which reflects whether or not end-on conversion occurred, is expected to be correlated with Mad2 loss. Indeed, the speed of kinetochore movement during 30 minutes after CENP-E reactivation was correlated with the rate of Mad2 loss (Fig. 2G), suggesting that the speed of congression initiation is dictated by the rate of formation of end-on attachments, which is reflected in the rate of Mad2 loss (Fig. 2H).

In the absence of CENP-E, the expansion of the fibrous corona inhibits the formation of end-on attachments and chromosome congression

What inhibits the initiation of chromosome congression in the absence of CENP-E? Based on previous studies (Cheerambathur et al., 2013), we hypothesized that the fibrous corona—a dense protein meshwork that forms on kinetochores in the absence of end-on microtubule attachments (Gassmann, 2023; McAinsh and Kops, 2023)—might play a role in this inhibition. To test if the corona inhibits congression, we compared the mean levels of CENP-E, used as a corona marker (Wu et al., 2023; Cmentowski et al., 2023) and Mad2 on kinetochores following CENP-E inhibition, CENP-E depletion (note that here Zw10 was used as a corona marker, see below), and in control cells (Fig. 3A). Our analysis revealed a strong correlation between Mad2 and CENP-E levels on polar kinetochores in both control and CENP-E-inhibited cells, which did not increase with saturating concentrations of CENP-E inhibitor (Fig. 3B and C). The average levels of both

proteins were significantly higher in CENP-E-inhibited cells compared to prometaphase cells (Fig. 3B and C), indicating excessive corona expansion on polar kinetochores following CENP-E inhibition. Surprisingly, in CENP-E-depleted cells, the level of Mad2 on polar kinetochores remained similar to that in CENP-E-inhibited cells despite a significant reduction in the amount of kinetochore CENP-E (Fig. 3B and C). In line with this, using Zw10, a component of the RZZ complex and a marker of the corona (Cmentowski et al., 2023; Sacristan et al., 2018), we observed excessive recruitment of Zw10 to polar kinetochores compared to control prometaphase cells, especially following CENP-E depletion (Fig. 3D-F). In contrast, the level of the outer kinetochore marker Mis12 on polar kinetochores remained unchanged on polar kinetochores following CENP-E perturbations (Fig. 3D-F). These findings suggest that without CENP-E or its activity, corona expands on polar kinetochores (Fig. 3G), contributing to the obstruction of end-on conversion (Cheerambathur et al., 2013) and chromosome congression.

Figure 3

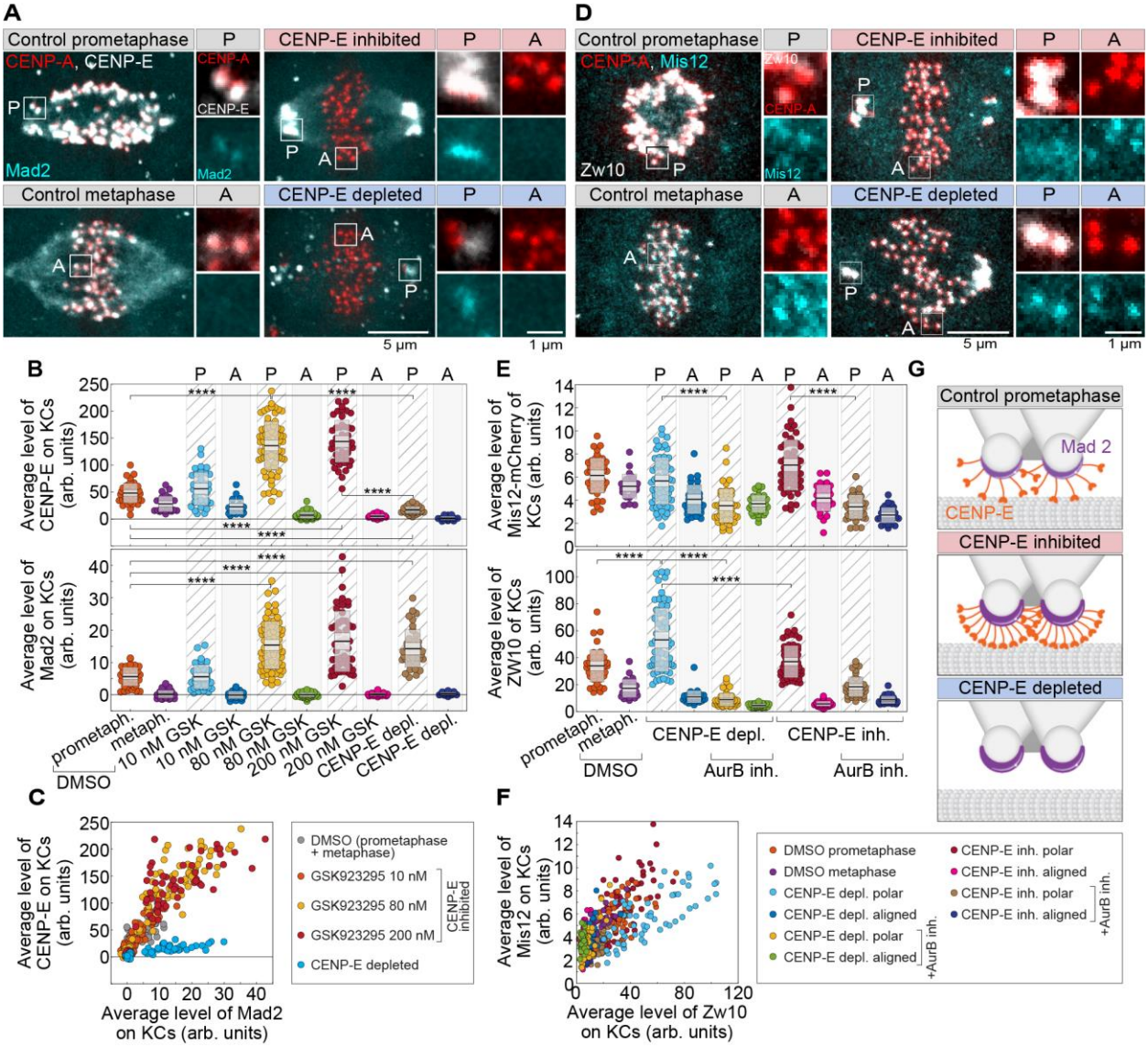

Figure 3. The fibrous corona expands on kinetochores in the absence of CENP-E or its activity, contributing to the inhibition of congression initiation. (A) Representative examples of cells expressing Mad2-mRuby (cyan) and CENPA-mCerulean (red) immunostained for CENP-E (grey) after the indicated treatments. Images are maximum intensity projections of merged channels (left) and enlarged kinetochore pairs per boxed area (right). A, aligned, P, polar. (B) Mean levels of CENP-E (top), and Mad2-mRuby (bottom) on kinetochores under the indicated treatments. GSK, GSK923295. (C) Average level of Mad2 on kinetochores versus average level of CENP-E on kinetochores in different treatments as per legend on the right. (D) Representative examples of cells expressing Mis12-mCherry (cyan) and CENP-A-GFP (red) immunostained for Zw10 (grey) after the indicated treatments. Images are maximum intensity projections of merged channels (left) and enlarged kinetochore pairs per boxed area (right). (E) Mean levels of Mis12-Mcherry (top), and Zw10 (bottom) under the indicated treatments. (F) Average level Zw10 on kinetochores versus average level of Mis12 on kinetochores in different treatments as per legend on the right. All images are a maximum projection of all acquired z planes. Numbers not given elsewhere: 53 cells, 744 kinetochores (B and C), 78 cells, 810 kinetochores (E and F), each from at least three independent biological replicates. (G) Diagrams showing the levels of CENP-E (orange) attached laterally to microtubules (grey tubule) and Mad2 (purple crescent) on polar kinetochores under the conditions indicated at the top. Symbols indicate: n.s. $P > 0.05$, $*P \leq 0.05$, $**P \leq 0.01$, $***P \leq 0.001$, $****P \leq 0.0001$. arb., arbitrary; inh., inhibited; depl, depleted; reac., reactivated; metaph., metaphase; prometaph., prometaphase; KC, kinetochore. Statistics: Tukey's HSD test.

Super-resolution microscopy reveals bioriented chromosomes near centrosomes after CENP-E reactivation

To directly test if congression is coupled with biorientation, we performed super-resolution imaging of spindle microtubules by using Stimulated Emission Depletion (STED) microscopy in CENP-E inhibited cells, and after reactivation of CENP-E at two time-points in RPE-1 and cancer osteosarcoma U2OS cells. This approach enabled us to observe and quantify different types of microtubule attachments to kinetochores during chromosome congression (Fig. 4A; and Fig. S3E). The reactivation of CENP-E was accompanied by chromosome congression and a gradual transition from lateral to end-on attachments on polar chromosomes in RPE-1 (Fig. 4A and B), and U2OS cells (Fig. S3E), while the attachment status on aligned kinetochores remained unchanged (Fig. 4C). The interkinetochore distance, along with the fraction of bioriented kinetochores, progressively increased with distance from the centrosome until reaching approximately 2.5 μm, at which point nearly all polar kinetochores were bioriented (Fig. 4D). In CENP-E-inhibited cells (Fig. S3E), congressing chromosomes situated between the metaphase plate and the spindle pole, which represented less than 5% of all polar chromosomes, were also bioriented and stretched (Fig. 4E). Collectively, our results demonstrate that chromosome movement during congression involves conversion from lateral to end-on kinetochore-microtubule attachments close to the spindle poles (Fig. 4F), with CENP-E playing an important role in accelerating this process.

Figure 4

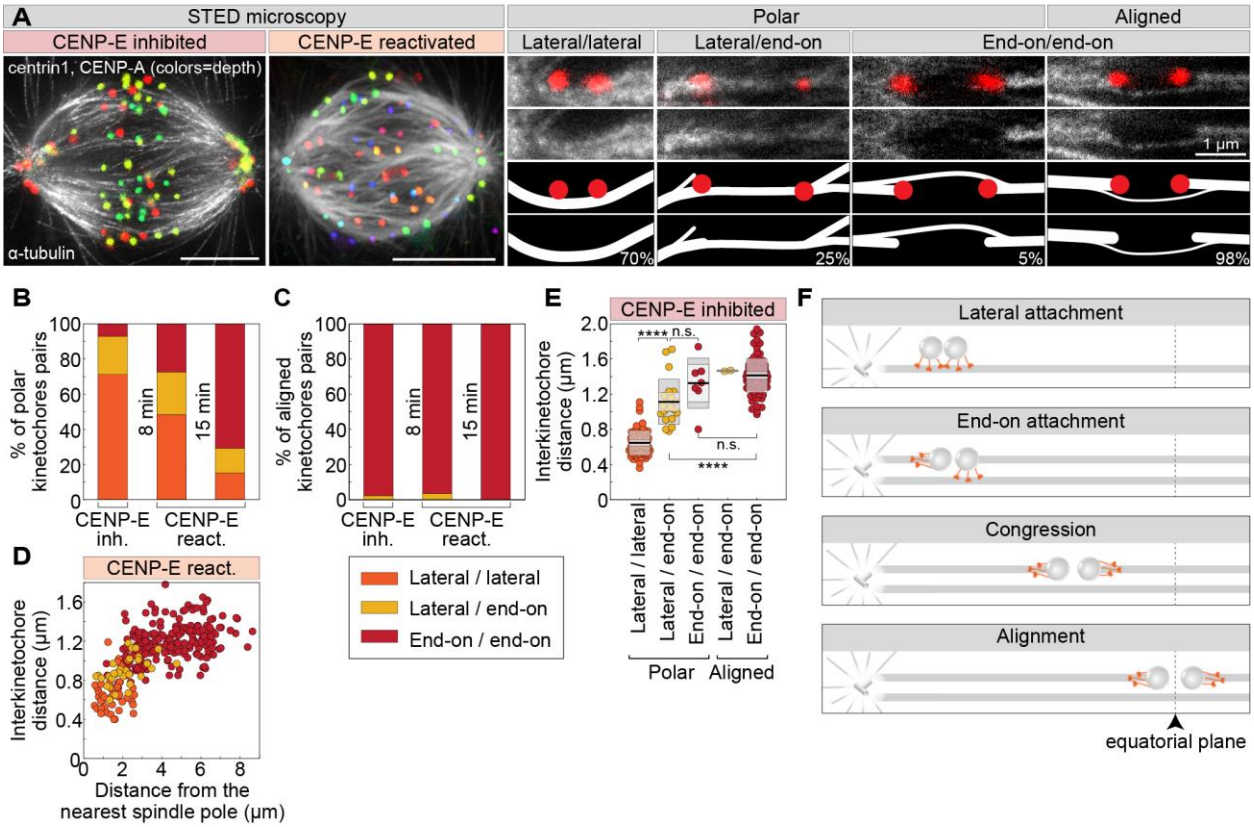

Figure 4. The initiation of chromosome congression near the centrosomes following CENP-E reactivation is accompanied by chromosome biorientation. (A) Representative examples of spindles after CENP-E inhibition (left spindle) or 15 minutes after CENP-E reactivation (right spindle) immunostained for α-tubulin and imaged by stimulated emission depletion (STED) microscopy in cells expressing CENP-A-GFP and centrin1-GFP. Projection is color coded by depth as specified by the color bar in 1A (left panel). Insets of kinetochore pairs with microtubules from different attachment categories, as depicted, from CENP-E inhibited cells, and schemes of microtubules (white) and kinetochores (red) of the respective insets (right panel). Percentages represent the proportion of each attachment category in cells with CENP-E inhibition. (B and C) Percentage of attachment categories indicated in the legend below across kinetochores per the indicated treatment groups for polar (B) and aligned (C) kinetochores. (D) Distance from the nearest spindle pole of kinetochore pair versus interkinetochore distance after CENP-E reactivation in the indicated attachment categories as per legend on the right. (E) Interkinetochore distances for indicated microtubule attachment categories across spindles treated with the CENP-E inhibitor. The black line shows the mean; the light and dark gray areas mark the 95% confidence intervals on the mean and standard deviation, respectively. (G) Diagrams showing that the transition from lateral to early end-on attachments precedes majority of the kinetochore movement toward the spindle equator and occurs near the spindle poles following CENP-E reactivation and in the absence of CENP-E. All images are a maximum projection of all acquired z planes. Numbers: 69 cells, 380 kinetochore pairs (B-D), 20 cells, 185 kinetochore pairs (E and F), each from at least three independent biological replicates. Statistics: Tukey's HSD test. Symbols

indicate: n.s. $P > 0.05$, *$P \leq 0.05$, **$P \leq 0.01$, ***$P \leq 0.001$, ****$P \leq 0.0001$. arb., arbitrary; inh., inhibited; react., reactivated.

Aurora kinases delay the initiation of congression in the absence of CENP-E activity

Having demonstrated that CENP-E promotes end-on attachments to initiate chromosome congression movement, we aimed to systematically explore the molecular pathways involved in the inhibition of congression in the absence of CENP-E activity through acute inhibition experiments targeting various molecules (Fig. 5A). We hypothesized that a signaling pathway inhibits the stabilization of end-on attachments in the absence of CENP-E, thereby preventing congression. Consequently, if end-on conversion is initiated in the absence of CENP-E activity, we would expect polar chromosomes to initiate congression. To test this, we inhibited Aurora B kinase that counteracts formation of end-on attachments (Shrestha et al., 2017), and maintenance of the Mad1:Mad2 as well as RZZ complex on kinetochores (Maia et al., 2010; Shrestha et al., 2017; Cheerambathur et al., 2013; Famulski and Chan, 2007). Fascinatingly, following acute inhibition of Aurora B with 3 µM ZM-447439 (Ditchfield et al., 2003) in both CENP-E-inhibited and depleted conditions, polar chromosomes immediately began moving, with most completing congression within 30 minutes after inhibitor addition (Fig. 5B-D, and Fig. S4A-F; and Video 5). A small fraction of polar chromosomes did not reach the metaphase plate but ended their journey close to the plate (Fig. 5B, arrows; and Fig. S4F), probably due to deficient correction of attachment errors (Lampson et al., 2004). These results imply that polar chromosomes initiate congression rapidly without CENP-E if end-on conversion is allowed by the acute inhibition of Aurora B.

Chromosome congression after acute inhibition of Aurora B in the absence of CENP-E activity was neither dependent on the premature onset of anaphase that was blocked by the usage of proteasome inhibitor MG132 (Santaguida et al., 2011) (Fig. S4G), nor the lower concentration (Fig. S4H) and specificity of Aurora B inhibitor (Yang et al., 2007) (Fig. S4I). Furthermore, the depletion of the cohesion release factor WAPL (Hengeveld et al., 2017) (Fig. S4J), the co-depletion of the chromokinesins Kid/kinesin-10 and Kif4a/kinesin-4 (Barisic et al., 2014) (Fig. 5C; and Fig. S4K), nor the acute inhibition of Protein phosphatases 1 and 2A (PP1/PP2A) by Okadaic acid (Su et al., 2016) (Fig. 5C; and Fig S4K and L) did not stop chromosomes from initiating and finishing congression after acute inhibition of Aurora B. This implies that the loss of centromeric cohesion (Hindriksen et al., 2017), the polar ejection forces generated by chromokinesins on chromosome arms (Drpic et al., 2015; Cane et al., 2013) and the activity of phosphatases (Ehlén et al., 2020) are not essential for congression movement after acute inhibition of Aurora B.

Interestingly, chromosome congression in the absence of both CENP-E and Aurora B activity was marked by rapid movement of polar kinetochores toward the equatorial plane, that was indistinguishable in velocity from other CENP-E perturbations (Fig. 5D and E; and Fig. S4A-B and M). However, a distinctive feature of congression without Aurora B activity was the absence of the slower initial phase of congression (Fig. S4A and B). This indicates that only the initiation of congression after CENP-E reactivation requires Aurora B activity, suggesting that CENP-E initiates chromosome congression by down-regulating Aurora B activity.

To gain further insight into the signaling mechanisms that limit chromosome congression in the absence of CENP-E, we co-inhibited or depleted various molecular regulators involved in biorientation or Aurora B recruitment (Ali and Stukenberg, 2023) under CENP-E inhibited condition. Interestingly, acute inhibition of Aurora A kinase, which shares specificity and certain kinetochore targets with Aurora B, most notably the kinetochore protein Hec1 (Highly expressed in cancer 1) (Ye et al., 2015) induced congression of polar chromosomes in the absence of CENP-E, although much slower than acute Aurora B inhibition (Fig. 5B-D; and Video 5). On the other hand, inhibition and co-inhibition of Bub1 (Budding uninhibited by benzimidazoles 1) or Haspin, factors essential for the recruitment of Aurora B to the outer and inner centromere, respectively (Dai et al., 2005; Kawashima et al., 2007; Broad et al., 2020; Hadders et al., 2020), did not induce chromosome congression in the absence of CENP-E activity, as well as inhibition of Polo-like kinase 1 (Plk1) kinase, and depletion of Bub1-related (BubR1) pseudokinase (Fig. 5C; and Fig. S4N). The only other kinase whose inhibition showed a minor but statistically nonsignificant effect compared to the control group was Monopolar spindle 1 (Mps1) kinase (Fig. 5C; and Fig. S4N). This implies that centrosome localized Aurora A and the outer-kinetochore localized Aurora B are major factors that limit the initiation of congression in the absence of CENP-E.

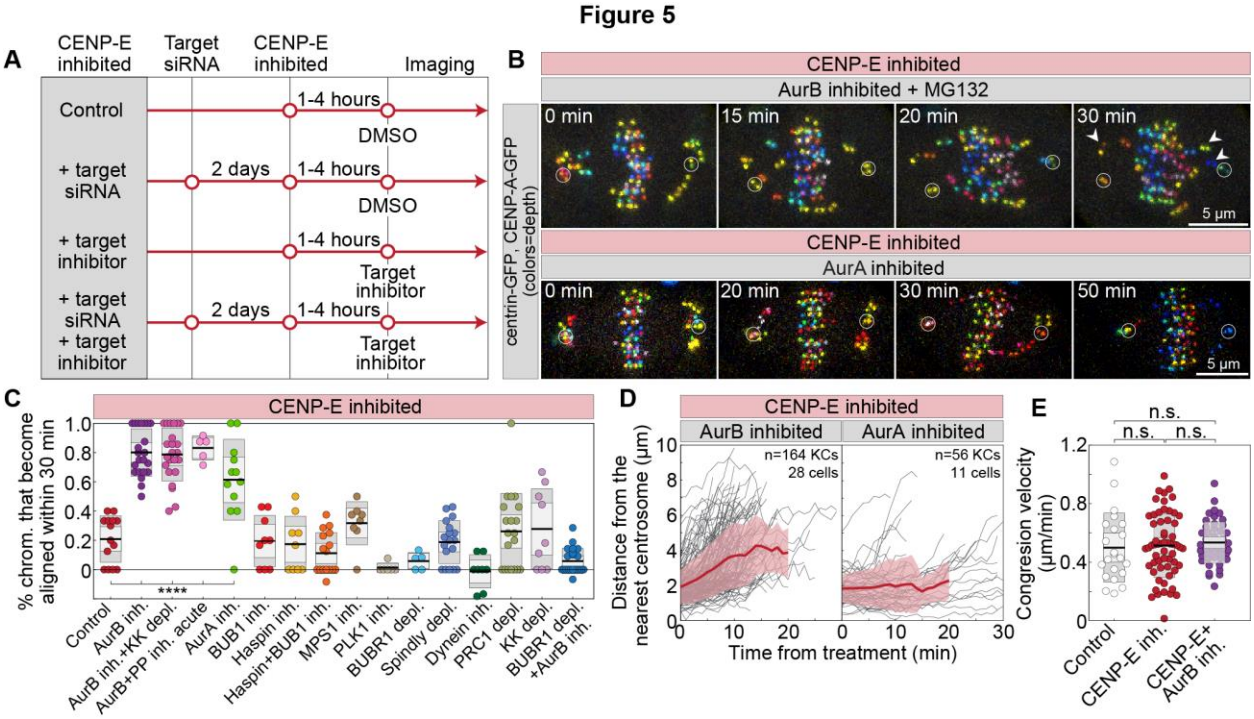

Figure 5. Aurora kinases inhibit chromosome congression in the absence of CENP-E. (A) Scheme of the experimental protocol to test which molecular factors limit chromosome congression in the absence of CENP-E activity. (B) Representative examples of cells expressing CENP-A-GFP and centrin1-GFP (denoted by white circles) in the presence of CENP-E inhibitor at different times after acute inhibition of target proteins as depicted. Time represents the time from the drug treatment. (C) Percentage of polar chromosomes that become aligned in the 30-minute period after indicated treatments in the presence of CENP-E inhibitor. The black line shows the mean; the light and dark grey areas mark the 95% confidence interval on the mean and standard

deviation, respectively. Numbers of cells per treatment: 14, 22, 23, 5, 12, 9, 9, 17, 8, 6, 5, 18, 8, 20, 9, 21, each from at least three independent experiments. Negative % means that more chromosomes were polar 30 minutes after CENP-E inhibition compared at the start of inhibition. (D) Distance to the nearest centrosome of initially polar kinetochore pairs in time from the indicated acute treatment. Thick lines represent means, and gray areas over means represent standard deviations. (E) Velocity of chromosome congression during the 6-minute period that precedes complete alignment for control, CENP-E inhibited and CENP-E and Aurora B co-inhibited cells. Statistics: Tukey's HSD test. Symbols indicate: ****$P \leq 0.0001$. Inh., inhibited; depl., depleted; siRNA, small interfering RNA; PP, protein phosphatases; KK, Kid and Kif4a; KC, kinetochore; NT, non-targeting; AurB, Aurora B; AurA, Aurora A.

The delay in the initiation of chromosome congression in the absence of CENP-E could be due to the dominant activity of other motor proteins in the spindle. However, perturbations of microtubule motor proteins, including dynein (Barisic et al., 2010; Gassmann et al., 2010; Firestone et al., 2012), as well as Kid, Kif4a, Eg5 and the crosslinker of antiparallel microtubules PRC1 (Kajtez et al., 2016; Polak et al., 2017) revealed that neither their indirect nor direct perturbations induced congression of polar chromosomes in the absence of CENP-E (Fig. 5C; and Fig. S4N and O). These results suggest, respectively, that the poleward pulling forces exerted by kinetochore dynein, the activity of chromokinesins, the distance between the plus ends of microtubules nucleated in one spindle half and the opposite spindle pole, and the thickness of antiparallel microtubule bundles to which kinetochores are initially laterally attached (Matković et al., 2022), are not major obstacles to congression in the absence of CENP-E activity. Instead, the primary barrier to congression without CENP-E is the activity of Aurora kinases.

To determine if BubR1, a known interactor of PP2A and CENP-E (Shrestha et al., 2017; Suijkerbuijk et al., 2012; Kruse et al., 2013; Legal et al., 2020), is required for the initiation of chromosome congression after Aurora B inhibition, we acutely inhibited Aurora B in cells lacking CENP-E and BubR1. Interestingly, in cells depleted of BubR1 and inhibited for CENP-E, the congression of polar chromosomes was completely halted following Aurora B inhibition, in contrast to cells with intact BubR1 (Fig. 5C). These results indicate that BubR1 is crucial for the initiation of chromosome congression, independent of its role in CENP-E recruitment (Legal et al., 2020), and that its absence cannot be compensated for by the inhibition of Aurora kinases.

Finally, we directly tested the role of corona expansion in inhibiting congression initiation in the absence of CENP-E by quantifying Zw10 levels on polar kinetochores following CENP-E perturbation and acute Aurora B kinase inhibition. We found that acute Aurora B inhibition caused a significant decrease in Zw10 levels on polar kinetochores, reducing them to levels similar to those observed on aligned kinetochores in the absence of Aurora B inhibition, both after CENP-E inhibition and depletion (Fig. 3E, F). These findings support our conclusion that kinetochore corona expansion, in the absence of CENP-E or its activity, contributes to the inhibition of chromosome congression initiation, and that this inhibition can be relieved by Aurora B inhibition.

CENP-E initiates chromosome congression in a manner that depends on BubR1

We next used the acute reactivation of CENP-E, combined with the acute inhibition of other target molecules, as a tool to identify which molecular factors regulate chromosome congression both upstream and downstream of CENP-E (Fig. 6A). As a first hypothesis, we assumed that the role of CENP-E in the initiation of chromosome congression reflects the recruitment of protein phosphatases to the outer kinetochore, either directly through interaction with PP1 or through its interaction with BubR1-PP2A (Kim et al., 2010; Song et al., 2021). However, acute or 30-minute long inhibition (see Methods) of PP1/PP2A activities by Okadaic acid did not prevent chromosome congression after reactivation of CENP-E (Fig. 6B and C; Fig. S5A and B; and Video 5), similarly to the finding that inhibition of PP1 in HeLa cells during prometaphase did not block congression of polar chromosomes (Kim et al., 2010). Congression after CENP-E reactivation was also successful without the activities of Plk1 kinase which regulates microtubule dynamics and recruits PP2A to BuBR1 (Salimian et al., 2011; Kruse et al., 2013), Kif18a/kinesin-8, which promotes chromosome alignment at the metaphase plate (Stumpff et al., 2008), or the chromokinesins Kid and Kif4a and thus the polar ejection forces they generate (Drpic et al., 2015) (Fig. 6C; and Fig. S5C).

Phosphorylation of CENP-E by Aurora kinases has previously been reported as crucial for CENP-E's motor activity and for the congression of polar chromosomes (Kim et al., 2010). However, polar chromosomes were still able to congress after reactivation of CENP-E when Aurora B kinase was acutely inhibited (Fig. 6D and E). Similar to the effect of acute Aurora B inhibition in the absence of CENP-E activity (Fig. 5B, arrows), congression following Aurora B inhibition in the presence of CENP-E activity was occasionally marked by incomplete congression of a minority of polar chromosomes (Fig. 6E, arrows). This suggests that issues with error correction, caused by Aurora B inhibition (Lampson et al., 2004), limit the complete congression of some polar chromosomes. In summary, polar chromosomes can initiate congression when Aurora B is fully inhibited, regardless of CENP-E activity.

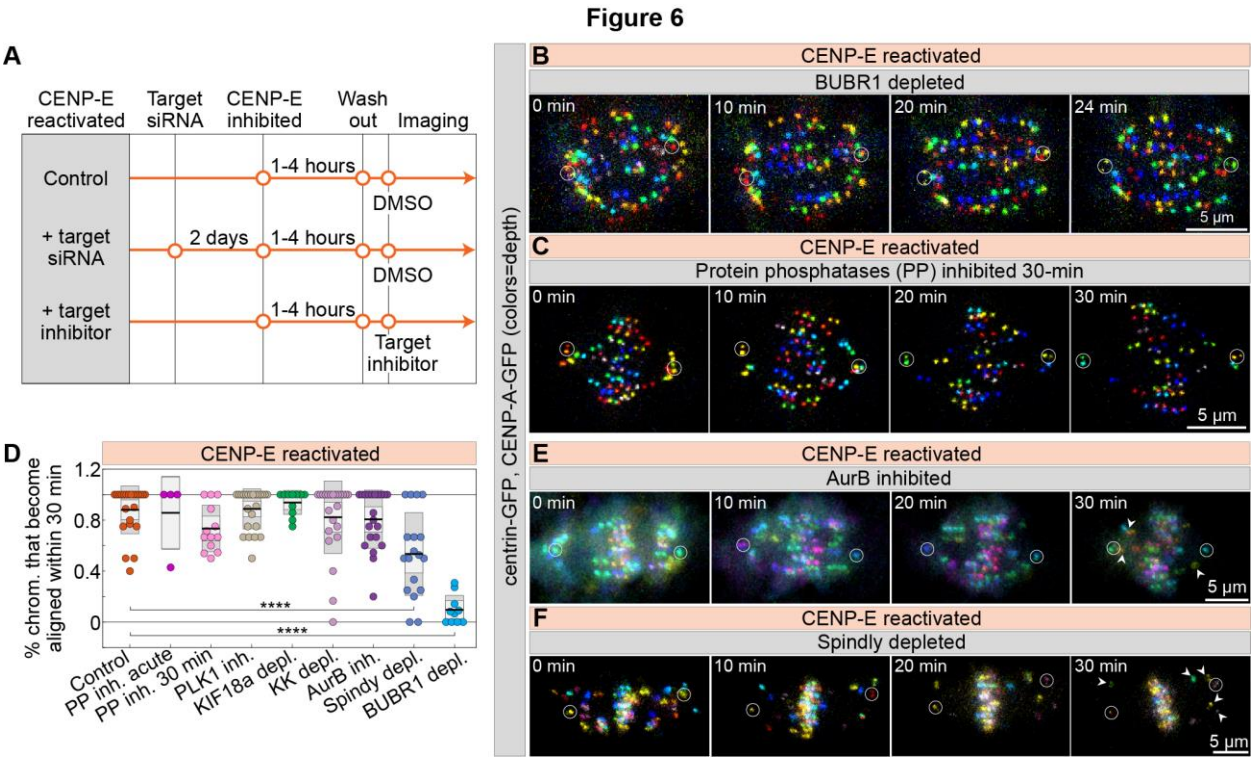

Figure 6. Lateral attachments and BubR1 are essential prerequisites for CENP-E-mediated chromosome congression. (A) Scheme of the experimental protocol to test which molecular factors regulate the congression of polar chromosomes after the reactivation of CENP-E activity by the wash-out of the CENP-E inhibitor. (B and C) Representative examples of cells expressing CENP-A-GFP and centrin1-GFP (centrioles encircled in white) at different times following wash-out of the CENP-E inhibitor in the BubR1-depleted (B) or protein phosphatases preinhibited (C) cells. Time represents the time from wash-out. (D) Percentage of polar chromosomes that become aligned in the 30-minute period after the wash-out of the CENP-E inhibitor in the indicated treatments. Numbers of cells per treatment: 23, 4, 13, 24, 11, 23, 21, 18, 10, each from at least three independent biological replicates. (D-E) Representative examples of RPE1 cells expressing CENP-A-GFP and centrin1-GFP (centrioles denoted by white circles) in different frames as depicted after washout of the CENP-E inhibitor and addition of 3 µM Aurora B inhibitor ZM447439 (D) or washout of the CENP-E inhibitor in cells depleted of Spindly (E). Images are maximum projections color-coded by depth as specified by the color bar in Figure 1A. Time represents the time from the onset of acute treatment. Arrowheads denote polar kinetochores that failed to congress to the metaphase plate. Statistics: Tukey's HSD test. Symbols indicate: ****$P \leq 0.0001$. Inh., inhibited; depl., depleted; siRNA, small interfering RNA; PP, protein phosphatases; KK, Kid and Kif4a; AurB, Aurora B; AurA, Aurora A.

It remains unclear whether CENP-E activity requires the presence of lateral attachments to mediate congression, as would be expected if CENP-E functions through the establishment of end-on attachments. To increase the number of polar chromosomes with prematurely stabilized end-

on attachments, we reactivated CENP-E in cells depleted of Spindly, a dynein adaptor at the kinetochore (Gassmann et al., 2010; Barisic et al., 2014). The proportion of polar chromosomes that congressed after CENP-E reactivation was significantly lower in Spindly-depleted cells compared to controls (Fig. 6C, F). This suggests that CENP-E cannot initiate the congression of polar kinetochores with stable end-on attachments, or that Spindly is required to recruit CENP-E to kinetochores, as recently reported (Cmentowski et al., 2023).

Finally, we tested the role of BubR1 in CENP-E-mediated congression of polar chromosomes by depleting BubR1, inhibiting CENP-E, and treating cells with MG132 to prevent the premature onset of anaphase (Lampson and Kapoor, 2005). Subsequent reactivation of CENP-E activity in BubR1-depleted cells did not result in the congression of polar chromosomes, unlike in cells with intact BubR1 (Fig. 6B, C; Fig. S5B; Video 5). This finding, along with our observation that BubR1 is required to counteract Aurora B independently of CENP-E recruitment (Fig. 5C), suggests that BubR1 is crucial for the initiation of chromosome congression.

CENP-E initiates chromosome congression in a manner dependent on Hec1 and the establishment of end-on attachments

To challenge our model that congression requires biorientation, we investigated whether CENP-E facilitates chromosome movement independently of end-on attachments in cells depleted of Hec1 and KifC1/HSET—a condition reported to permit chromosome pseudoalignment without end-on attachments (Cai et al., 2009). We then combined this approach with CENP-E perturbations and analyzed chromosome alignment and Hec1 kinetochore levels in individual mitotic cells using immunofluorescence. Our results show that chromosome alignment improved after HSET depletion in Hec1-depleted cells, while additional CENP-E depletion led to severe misalignment (Fig. 7A, B), consistent with previous findings (Cai et al., 2009). Notably, the degree of chromosome alignment strongly correlated with the residual levels of Hec1 at the kinetochores, which were generally higher in Hec1- and HSET-codepleted cells compared to Hec1 depletion alone (Fig. 7C-E; Fig. S5D). Importantly, cells with minimal Hec1 at the kinetochores exhibited significant misalignment, regardless of HSET or CENP-E codepletion (Fig. 7A). In line with this, the movement of polar chromosomes in live-imaged Hec1-depleted cells was unaffected by CENP-E activity, as chromosome movement was similar in both Hec1-depleted and Hec1-depleted/CENP-E-inhibited cells (Fig. 7F), consistent with previous observations in HeLa cells (Iemura and Tanaka, 2015). These findings suggest that a minimal level of Hec1, about 10-15% of control levels, is sufficient to promote congression, and that CENP-E's role in chromosome congression is enhanced by the presence of Hec1.

Figure 7

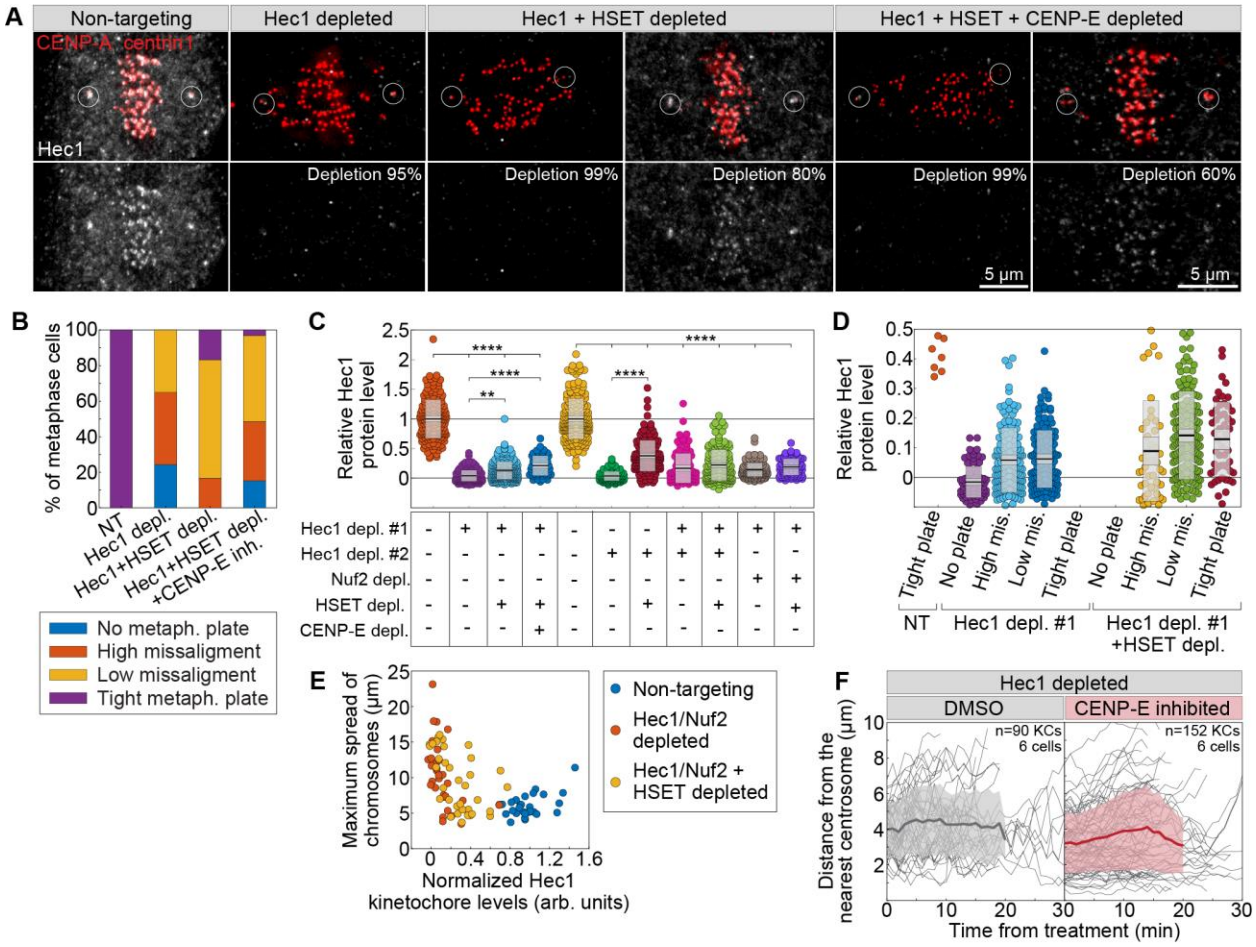

Figure 7. CENP-E has limited ability to drive chromosome movement when end-on attachment formation is compromised. (A) Representative examples of cells expressing CENP-A-GFP and centrin1-GFP (grey) immunostained for Hec1 (grey), with circled centrioles, in the treatments indicated on top. (B) Percentage of metaphase cells in the denoted treatments with different extent of chromosome misalignments as per legend on the top. (C and D) Average level of Hec1 on kinetochores normalized to the average of the non-targeting group over treatments (C) and over treatments and different alignment categories together as indicated at the bottom (D). Numbers: 1668 kinetochores from 153 cells (C), 733 kinetochores from 64 cells (D), all from at least three independent biological replicates. (E) Average Hec1 kinetochore levels normalized to non-targeting group average versus the maximum spread of chromosomes in each cell across different treatments as per legend on the right. Numbers: 31, 27, 24, 33 cells per treatment (B), 97 cells in total (E), each treatment done in at least three independent biological replicates. (F) Distance to the nearest centrosome of initially polar kinetochores in time for the treatments indicated on top. All images are maximum projections. Inh., inhibited; depl., depleted; metaph, metaphase; NT, non-targeting.

DISCUSSION

For nearly two decades, the model proposing that chromosomes are transported to the spindle equator without biorientation by kinetochore molecular motors like CENP-E has stood the test of time and remained unchallenged (Kapoor et al., 2006), inspiring many exciting models of chromosome movement and its regulation (Barisic et al., 2014, 2015; Cai et al., 2009; Kim et al., 2010; Eibes et al., 2023; Gudimchuk et al., 2013). Here, we present systematic evidence supporting an alternative model where the major part of chromosome movement during congression depends on biorientation, aligning with pioneering propositions on the topic (McEwen et al., 2001, 1997). In this model, CENP-E enhances the formation or stabilization of end-on attachments on polar chromosomes, thereby promoting rapid biorientation close to centrosomes and synchronous chromosome congression during early mitosis (Fig. 8A). These conclusions are based on the following results: 1) major part of chromosome congression movement has the same dynamics regardless of CENP-E presence or activity; 2) end-on attachments form and the Mad2 signal start to drop on polar kinetochores prior to their fast movement toward equatorial plane; 3) all congressing chromosomes are bioriented a few microns from the centrosome, as visualized by STED microscopy; 4) CENP-E has limited ability to drive chromosome movement without end-on attachments or if these attachments are prematurely stabilized close to pole; 5) congression initiates without CENP-E if Aurora kinases are inhibited, which forces chromosome biorientation; 6) BubR1 is essential for chromosome congression, regardless of its role in CENP-E recruitment.

We propose that the primary barrier to the initiation of congression in the absence of CENP-E is the activity of Aurora B kinase (Fig. 8B). Aurora B limits end-on attachment stability by phosphorylating KMN network components (DeLuca et al., 2011; Shrestha et al., 2017) and regulating the RZZ complex and fibrous corona expansion (Famulski and Chan, 2007; Cheerambathur et al., 2013) (Fig. 8B). Aurora A also directly phosphorylates KMN near centrioles (Ye et al., 2015). The activity of Aurora kinases, along with back-to-back kinetochore organization (Lončarek et al., 2007), prevents premature erroneous end-on attachments near centrosomes (Ye et al., 2015; Barisic et al., 2014) that could impede congression. Aurora kinases also phosphorylate and activate CENP-E near centrioles (Kim et al., 2010; Eibes et al., 2023) (Fig. 8B). We speculate that the activated CENP-E interacts with BubR1-PP2A (Huang et al., 2019) (Fig. 8B), and activity of PP2A leads to downregulation of Aurora B kinase activity, and net dephosphorylation of its substrates at the outer kinetochore. This stabilization of early end-on attachments on polar kinetochores, indicated by the onset of Mad2 loss, initiates congression movement (Fig. 8B). However, acute phosphatase inhibition and Plk1 inhibition experiments, which should inhibit phosphatase activity through BubR1 (Kruse et al., 2013), did not prevent efficient chromosome congression, suggesting that phosphatases are not essential for congression. Utilizing separation-of-function mutants of CENP-E and BubR1 could resolve this issue. Recent studies have shown that CENP-E exists in distinct pools on the kinetochore and fibrous corona (Cmentowski et al., 2023), with BubR1 and the RZZ complex recruiting these pools, respectively (Legal et al., 2020; Cmentowski et al., 2023; Weber et al., 2024). Since congression initiation depends on BubR1, we propose that it is primarily driven by the kinetochore-localized CENP-E.

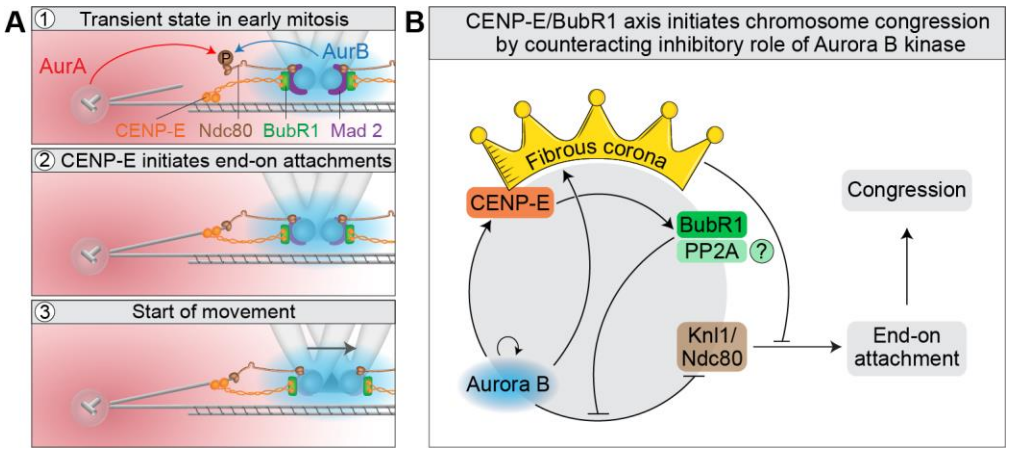

Figure 8. Model of chromosome congression regulation featuring a negative feedback loop between Aurora B kinase and CENP-E/BubR1. (A) Diagrams illustrating how Aurora kinases oppose congression initiation by phosphorylating Ndc80 tail close to the centrosomes (1); CENP-E-BubR1 facilitates the establishment of early end-on attachments near the Aurora A gradient on polar kinetochores, leading to drop in Aurora B activity on kinetochore, initiation of Mad2 loss from the kinetochore and stable Ndc80 binding on microtubule (2), all occurring before the onset of fast kinetochore movement (3). (B) Functional negative feedback loop of signaling interactions involving Aurora B kinase, CENP-E, BubR1-PP2A, fibrous corona, and outer-kinetochore proteins Knl1/Hec1 (KNL/Ndc80) that governs the formation of end-on attachments and the initiation of chromosome congression. Lines with arrows indicate activation, and blunt lines indicate deactivation. Polar chromosomes initially exhibit lateral attachments of kinetochores to microtubules, which fail to quickly convert to stable end-on attachments without CENP-E due to the high activity of outer-kinetochore localized Aurora B (AurB). AurB phosphorylates outer kinetochore proteins like Knl1 and Hec1 (Ndc80), essential for end-on attachment of microtubules to the outer kinetochore, and maintains the expanded fibrous corona (depicted as a crown) that inhibits end-on conversion and chromosome congression. Aurora B kinase also activate CENP-E by phosphorylation. We speculate (question mark sign) that the interaction of activated CENP-E with BubR1 and possibly protein phosphatase 2A (PP2A) is required to counteract Aurora B-mediated phosphorylation of outer kinetochore substrates. This stabilizes initial end-on attachments, initiating gradual end-on conversion and leading to subsequent congression movement of the chromosome towards the spindle midplane.

We propose that in addition to phosphorylating KMN network components, Aurora kinases inhibit the stabilization of end-on attachments by promoting the expansion of the fibrous corona on unattached chromosomes (Fig. 8B). Previously, it was proposed that competition between corona components and Ndc80 regulates microtubule engagement and end-on conversion (Cheerambathur et al., 2013). Recent studies indicate that CENP-E is crucial for expanding the fibrous corona (Wu et al., 2023; Cmentowski et al., 2023) which can nucleate and sort microtubules (Renda et al., 2022; Wu et al., 2023) or serve as a hub for capturing microtubules (Sacristan et al., 2018). However, our results, obtained in the presence of formed spindles, unlike

previous studies with depolymerized microtubules, demonstrate that the corona expands without CENP-E or its activity. Instead, we suggest that corona expansion inhibits end-on attachments and chromosome congression in the absence of CENP-E, supported by our and previous observations that corona is almost completely removed upon acute Aurora B inhibition (Famulski and Chan, 2007). However, our results show that Spindly removal in CENP-E perturbed cells is insufficient to initiate congression. Similarly, acute inhibition of Mps1, a key regulator of corona assembly (Sacristan et al., 2018), has a less pronounced effect on congression initiation compared to the inhibition of Aurora kinases. These results suggest that the expansion of the fibrous corona has a secondary effect in preventing end-on attachments compared to the phosphorylation of the KMN network.

Our model predicts that chromosome congression can initiate without CENP-E activity if the KMN network has maximum microtubule affinity, and the fibrous corona disassembles. We have shown that this occurs for polar chromosomes after acute inhibition of Aurora kinases. The presented model aligns with observations that constitutively dephosphorylated Hec1 does not interfere with congression, as the KMN network has maximum microtubule affinity under this condition (DeLuca et al., 2011; Etemad et al., 2015), akin to inhibition of Aurora kinases, and that congression resolves lateral attachments in bipolar spindles induced by forced localization of Aurora B on the outer kinetochore (Shrestha et al., 2017).

We do not exclude the possibility that CENP-E can facilitate chromosome movement by gliding polar kinetochores, if they are very close to the pole, along highly detyrosinated microtubules away from the Aurora A gradient (Barisic et al., 2014, 2015). However, chromosomes rarely encounter a high Aurora A gradient during unperturbed mitosis in healthy cells, as they do not approach the centrosomes (Renda et al., 2022; Magidson et al., 2011). This contrasts sharply with cancer cells, where some chromosomes come close to centrosomes early in mitosis, leading to congression delays (Klaasen et al., 2022). We propose that in healthy cells, the avoidance of regions near the centrosome by chromosomes may play a pivotal role in enabling rapid biorientation and congression. In the accompanying manuscript (Vukušić & Tolić, 2024), we provide evidence that centrosomes deliver a crucial spatial signal that determines the need for CENP-E during chromosome congression, as CENP-E counteracts the combined activity of Aurora kinases to initiate chromosome movement.

The coupling between mechanisms governing chromosome congression and chromosome biorientation has remained unclear to date. Previous models of chromosome movement suggested that kinetochore biorientation and chromosome congression are largely uncoupled processes (Barisic et al., 2014; Kapoor et al., 2006; Maiato et al., 2017), and that chromosomes take either biorientation or CENP-E-mediated routes of congression, implying two distinct mechanisms (Maiato et al., 2017). Here, we show that chromosome congression is coupled to biorientation through CENP-E (Fig. 8B), thereby proposing a unified model of congression movement. The notion that CENP-E is involved in end-on conversion has been proposed earlier, in particular that CENP-E maintains lateral attachments (Shrestha and Draviam, 2013). However, our findings suggest that CENP-E may directly promote end-on conversion and biorientation independently of gliding or stabilizing lateral attachments. Different roles of CENP-E independent of gliding were

proposed previously (Barisic and Rajendraprasad, 2021; Sikirzhytski et al., 2018; Gudimchuk et al., 2013), but their contribution to chromosome congression remains to be further explored. The model proposed in this and accompanying manuscript (Vukušić & Tolić, 2024) offers a molecular mechanism for the spatial and temporal coordination between biorientation and congression, involving the coupling of Aurora kinases, CENP-E, and BubR1 as major drivers or regulators of both processes (Fig. 8B) (Lampson and Kapoor, 2005; Barisic et al., 2014; Shrestha et al., 2017; Huang et al., 2019; Kim et al., 2010).

ACKNOWLEDGEMENTS

We thank Alexey Khodjakov and Jonathon Pines for cell lines; Marin Barišić, Carlos Conde, Helder Maiato and Andrea Musacchio for reviewing and discussing the manuscript; Julie Welburn for discussions and antibodies; Magda Topić and Mia Crnogaj for help with cell culture work and preparation of inhibitors; Ivana Šarić for the drawings; and members of the Tolić group and Nenad Pavin group for constructive comments on the manuscript. This work was funded by the European Research Council (ERC Synergy Grant, GA Number 855158), the Croatian Science Foundation (HRZZ) through Swiss-Croatian Bilateral Projects (project IPCH-2022-10-9344), and projects co-financed by the Croatian Government and the European Union through the European Regional Development Fund—the Competitiveness and Cohesion Operational Programme: IPSted (Grant KK.01.1.1.04.0057) and QuantiXLie Center of Excellence (Grant KK.01.1.1.01.0004).

AUTHOR CONTRIBUTIONS

K.V. and I.M.T conceived the project, K.V. performed all experiments, quantified, analyzed and presented the data, K.V. conceptualized and prepared original draft, K.V. and I.M.T. reviewed, edited and discussed the manuscript.

MATERIALS & METHODS

Reagents and Tools table

Reagent/Resource	Reference or Source	Identifier or Catalog Number
Experimental Models		
hTERT-RPE1 cells stably expressing CENP-A-GFP, human hTERT-RPE1	Alexey Khodjakov Lab, Wadsworth Center	N/A
hTERT-RPE1 cells stably expressing both CENP-A-GFP and centrin1-GFP	Alexey Khodjakov Lab, Wadsworth Center	N/A
hTERT-RPE1 cells stably expressing CENP-A-GFP and Mis12-mCherry	Alexey Khodjakov Lab, Wadsworth Center	N/A
hTERT-RPE1 cells stably expressing CENP-A-mCerulean and Mad2-mRuby	Jonathon Pines Lab, Institute for Cancer Research	N/A
Antibodies		
Rabbit monoclonal Anti-NDC80	Sigma-Aldrich	HPA066330
Mouse monoclonal anti-KIFC1 (M-6)	Santa Cruz	sc-100947
Rabbit polyclonal anti-Kif18a	Bethyl Laboratories	A301-080A
Rabbit anti-Kif4A	Bethyl Laboratories	A301-074A
Rabbit anti-SPINDLY/CCD98	Bethyl Laboratories	A301-354A
Mouse monoclonal anti-KID (B-9)	Santa Cruz	sc-390640
Rat anti-alpha-tubulin YL1/2	Invitrogen	MA1-80017
Donkey anti-rabbit IgG Alexa Fluor 647	Abcam	ab150075
Donkey anti-rabbit IgG Alexa Fluor 594	Abcam	ab150064
Donkey anti-mouse IgG Alexa Fluor 594	Abcam	ab150108

Donkey anti-mouse IgG Alexa Fluor 647	Abcam	ab150107
Donkey anti-rat IgG Alexa Fluor 594	Abcam	ab150156
Oligonucleotides and other sequence-based reagents		
human CENP-E ON-TARGETplus SMART pool siRNA	Dharmacon	L-003252-00-0010
human PRC1 ON-TARGETplus SMART pool siRNA	Dharmacon	L-019491-00-002
human custom-made Ndc80/Hec1 siRNA, oligo #1	Dharmacon	sequence: 5'-GAAUUGCAGCAG ACUAUUA-3'
human MISSION esiRNA kntc2 (NDC80), oligo #2	Merck	EHU042171-20UG
human ON-TARGETplus SMART pool NUF2 siRNA	Dharmacon	L-005289-00-000
human custom-made 3'UTR HEC1 siRNA, oligo #3	Thermo Fisher Scientific	sequence 5′-CCCUGGGUCGUG UCAGGAA-3′
human ON-TARGETplus SMART pool KIFC1 (HSET) siRNA	Dharmacon	L-004958-0010
human KIF4A siRNA	Santa Cruz Biotechnology	sc-60888
human Kif18A siRNA	Ambion	#Cat 4390825, ID:s37882
human Kif22/Kid siRNA	Ambion	#Cat 4392420, ID:s7911
human WAPL ON-TARGETplus SMART pool siRNA	Dharmacon	J-026287-10-0010
human BUB1B/BuBR1 ON-TARGETplus SMART pool siRNA	Dharmacon	L-004101-00-0005
human custom-made Spindly siRNA	Sigma-Aldrich	Sequence antisense: 5'-GAAAGGGUCUCA

		AACUGAA-3', dTdT overhangs
control siRNA	Dharmacon	D-001810-10-05
Chemicals, Enzymes and other reagents		
MG-132	Merck	M7449
Lipofectamine RNAiMAX Reagent	Thermo	13778150
OPTI-MEM medium	Thermo	31985062
DMEM medium	Thermo	11995065
Barasertib	Selleckchem	S1147
GSK-923295	MedChemExpress	HY-10299
Monastrol	MedChemExpress	HY-101071A
ZM-447439	MedChemExpress	HY-10128
MLN8237	MedChemExpress	HY-10971
BAY-320	MedChemExpress	HY-104000
5-Iodotubercidin	MedChemExpress	HY-15424
AZ3146	MedChemExpress	HY-14710
BI 2536	MedChemExpress	HY-50698
Okadaic acid	MedChemExpress	HY-N6785
Ciliobrevin D	MedChemExpress	HY-122632
Fetal bovine serum (FBS)	Thermo-Fisher	10270106
µ-Dish 35 mm, high Glass Bottom	Ibidi	81158
35 mm Dish 1.5 Coverslip 10 mm Glass Diameter Uncoated	Mattek	P35G-1.5-10-C
Software		
ImageJ (Fiji)	https://imagej.net/software/fiji/	N/A
Prairie View Imaging Software	Bruker	N/A
Imspector software	Abberior	N/A
ZEN 2.6 software	Zeiss	N/A
MatlabR2021a	MathWorks	
Matlab extension UnivarScatter	https://github.com/manulera/UnivarScatter	N/A

Matlab Statistics Toolbox R14	MathWorks	N/A
Adobe Illustrator CS6	Adobe Systems	N/A
Low Light Tracking Tool (v.0.10) ImageJ plugin	https://imagej.net/plugins/low-light-tracking-tool	N/A
Other		
Opterra I multipoint scanning confocal microscope system	Bruker	N/A
Expert Line easy3D STED microscope system	Aberior	N/A
LSM 800 confocal laser scanning microscope system	Zeiss	N/A
Lattice Lightsheet 7 microscope system	Zeiss	N/A

Methods and Protocols

Cell lines and culture

Experiments were carried out using human hTERT-RPE1 (hTERT-immortalized retinal pigment epithelium) cells stably expressing CENP-A-GFP, human hTERT-RPE1 cells stably expressing both CENP-A-GFP and centrin1-GFP and human hTERT-RPE1 cells stably expressing CENP-A-GFP and Mis12-mCherry, all courtesy of Alexey Khodjakov (Wadsworth Center, New York State Department of Health, Albany, NY, USA), human hTERT-RPE1 cells stably expressing CENP-A-mCerulean and Mad2-mRuby, courtesy of Jonathon Pines (Institute of Cancer Research, London, UK), and human HeLa (cervical carcinoma patient) cells expressing GFP-Hec1-9A, courtesy of Geert Kops (Hubrecht Institute, Utrecht, The Netherlands) . All cell lines were cultured in flasks in Dulbecco's Modified Eagle's Medium with 1 g/L D-glucose, pyruvate and L-glutamine (DMEM, Thermo Fisher, 11995065), supplemented with 10% (vol/vol) heat-inactivated Fetal Bovine Serum (FBS, Sigma-Aldrich, St. Louis, MO, USA) and penicillin (100 IU/mL)/streptomycin (100 mg/mL) solution (Lonza, Basel, Switzerland). The cells were kept at 37 °C and 5% CO2 in a humidified incubator (Galaxy 170 S CO2, Eppendorf, Hamburg, Germany) and regularly passaged at the confluence of 70-80%. None of the cell lines were authenticated. All cell lines have also been tested for mycoplasma contamination once a month by examining samples for extracellular DNA staining with SiR-DNA (100 nM, Spirochrome, Stein am Rhein, Switzerland) and Hoechst 33342 dye (1 drop/2 ml of NucBlue Live ReadyProbes Reagent, Thermo Fisher Scientific, Waltham, MA, USA) and have been confirmed to be mycoplasma free.

Sample preparation and siRNAs

At 80% confluence, the DMEM medium was removed from the flask and the cells were washed with 5 ml of phosphate buffered saline (PBS). Then, 1 ml 1% trypsin/ethylenediaminetetraacetic acid (EDTA, Biochrom AG, Berlin, Germany) was added to the flask and cells were incubated at 37 °C and 5% CO_2 in a humidified incubator for 5 min. After incubation, trypsin was blocked by adding 4 ml of DMEM medium. For the RNAi experiments, cells were seeded to reach 60% confluence the next day and cultured on 35 mm uncoated plates with 0.17 mm (#1.5 coverglass) glass thickness (MatTek Corporation, Ashland, MA, USA) in 1 ml of DMEM medium with the supplements described above. After one day of growth, cells were transfected with either targeting or non-targeting siRNA constructs which were diluted in OPTI-MEM medium (Thermo-Fisher) to a final concentration of 100 nM in the medium with cells. All transfections were performed 48 h before imaging using Lipofectamine RNAiMAX Reagent (Life Technologies, Waltham, MA, USA) according to the instructions provided by the manufacturer, unless otherwise indicated. Codepletions of Hec1 or Nuf2 and HSET and CENP-E in RPE-1 cells were performed for two times in two subsequent days by the same protocol. After four hours of siRNA treatment, the medium was changed to the prewarmed DMEM medium. Proteasome inhibitor MG-132 (Merck, M7449, IC50 value 100 nM) was used at a final concentration of 1 μM where indicated.

The siRNA constructs used were: human CENP-E ON-TARGETplus SMART pool siRNA (L-003252-00-0010, Dharmacon, Lafayette, CO, USA), human PRC1 ON-TARGETplus SMART pool siRNA (L-019491-00-0020, Dharmacon), human custom-made Ndc80/Hec1 siRNA (oligo #1, sequence: 5'- GAAUUGCAGCAGACUAUUA-3', Dharmacon), human MISSION esiRNA kntc2 (NDC80) (oligo #2, EHU042171-20UG, Merck), human ON-TARGETplus SMART pool NUF2 siRNA (L-005289-00-000, Dharmacon), human ON-TARGETplus SMART pool KIFC1 (HSET) siRNA (L-004958-0010, Dharmacon), human KIF4A siRNA (sc-60888, Santa Cruz Biotechnology), human Kif18A siRNA (Ambion, #Cat 4390825, ID:s37882), human Kif22/Kid siRNA (Ambion, #Cat 4392420, ID:s7911), human WAPL ON-TARGETplus SMART pool siRNA (J-026287-10-0010, Dharmacon), human BUB1B/BuBR1 ON-TARGETplus SMART pool siRNA (L-004101-00-0005, Dharmacon, Lafayette, CO, USA), human Spindly siRNA (Sequence antisense: 5'- GAAAGGGUCUCAAACUGAA-3', dTdT overhangs, Sigma-Aldrich, St. Louis, MO, USA), and control siRNA (D-001810-10-05, Dharmacon, Lafayette, CO, USA).

Drug treatments and drug washouts

Aurora B inhibitor Barasertib (AZD1152-HQPA, Selleckchem, Munich, Germany, IC_{50} value 0.32 nM) at a final concentration of 300 nM, was added acutely before imaging. CENP-E inhibitor GSK-923295 (MedChemExpress, Monmouth Junction, NJ, USA, IC50 value 3.2 nM) at a final concentration of 80 nM for RPE-1 and 200 nM for U2OS, to achieve the same effect, was added 1-4 hours before imaging in most experiments, or when noted acutely before imaging. Eg5 inhibitor Monastrol (HY-101071A/CS-6183, MedChemExpress, IC_{50} value 50 μM) at a final concentration of 100 μM, was added 3 hours before imaging or acutely before imaging when noted. Aurora B inhibitor ZM-447439 (MedChemExpress, IC_{50} value 130 nM) at a final concentration of 2 or 3 μM as noted, was added acutely before live imaging or 15 minutes before fixation as noted. Aurora A inhibitor MLN8237 (MedChemExpress, IC_{50} value 4 nM) at a final final concentration of 125 nM or 250 nM as noted, was added acutely before imaging or 30-60 minutes before fixation.

Bub1 inhibitor BAY-320 (MedChemExpress, IC_{50} value 680 nM) at a final concentration of 10 μM, was added acutely before imaging. Haspin inhibitor 5-Iodotubercidin (5-ITu) (MedChemExpress, IC_{50} value 5-9 nM) at a final concentration of 2 μM, was added acutely before imaging. Mps1 inhibitor AZ3146 (MedChemExpress, USA, IC_{50} value 35 nM) at a final concentration of 500 nM, was added acutely before imaging. PLK1 inhibitor BI 2536 (MedChemExpress, IC_{50} value 0.83 nM) at a final concentration of 100 nM, was added acutely before imaging. Inhibitor of PP1 and PP2A Okadaic acid (MedChemExpress, IC_{50} value 0.1-0.3 nM for PP2A and 15-50 nM for PP1) at a final concentration of 1 μM, was added acutely before imaging or 30 minutes before washout of the CENP-E inhibitor as noted. Cytoplasmic dynein inhibitor Ciliobrevin D (MedChemExpress) at a final concentration of 20 μM, was added acutely before imaging. Proteasome inhibitor MG-132 (Merck, IC_{50} value 100 nM) at a final concentration of 1 μM, was added acutely before imaging or together with CENP-E inhibitor as noted.

The stock solutions for all drugs were prepared in DMSO except Okadaic acid which was prepared in ethanol. The stock solutions of all drugs were kept aliquoted at 10-50 μL at -20 °C for a maximum period of three months or at -80 °C for a maximum period of six months. New aliquots were thawed weekly for each new experiment. All drugs were added to DMEM media used for cell culture to obtain the final concentration of a drug as described, except Ciliobrevin D, which was added to a serum-reduced Opti-MEM medium that was placed on cells acutely before adding the drug, as Ciliobrevin D did not show any effect when used in DMEM medium with 10% FBS (Firestone et al., 2012). Drug washouts were performed by replacing drug-containing medium with 2 mL of fresh pre-warmed DMEM medium followed by four subsequent washouts with 2 mL of pre-warmed DMEM.

Acute inhibition of Aurora B by ZM-447439 (2 or 3 μM) or barasertib (300 nM) induced premature anaphase onset 15-30 min after the addition of Aurora B inhibitor, as reported previously (Maia et al., 2010). Similarly, premature onset of anaphase was observed during the 30 min course of the imaging in cells acutely treated with the Mps1 inhibitor AZ3146 (500 nM), as expected from previous work (Santaguida et al., 2011). When noted in the text, we treated CENP-E inhibited cells with the proteasome inhibitor MG-132 together with Aurora B or Mps1 inhibitors to block premature anaphase onset. MG-132 treatment provided more time for the chromosomes to complete the alignment successfully, as in the Aurora B inhibitor alone, anaphase ensued while some chromosomes were still in the alignment process.

Acute treatment of cells with dynein inhibitor 20 μM Ciliobrevin D splayed the spindle poles in all treated cells during 30 minutes after the addition of the drug, reflecting the reported role of the dynein-dynactin complex in the focus of the spindle poles in human cells (Firestone et al., 2012). Interestingly, co-inhibition of Bub1 by BAY-320 (10 μM) and Haspin by 5-ITu (2 μM) in some cells induced premature onset of anaphase during the first 20 minutes after addition of the drug, reflecting the possible role of both pathways in the maintenance of the spindle assembly checkpoint (Hengeveld et al., 2017). 30-minute long Okadaic acid treatment (1 μM) led to depolymerization of actin filaments and rounding of interphase cells (Fiorentini et al., 1996). Acute treatment of cells with Okadaic acid (1 uM) together with acute treatment with Aurora B inhibitor or after CENP-E inhibitor washout resulted in frequent expels of aligned kinetochores from the

plate and sometimes complete breakage of the integrity of metaphase plates, but only after most of the polar chromosomes had already aligned to the plate, similar to previous reports of PP1 antibody injections into HeLa cells (Kim et al., 2010). After acute treatment of CENP-E inhibited cells with the Eg5 inhibitor monastrol (50 uM), spindles quickly shortened, as expected from previous reports (Vukušić et al., 2021). Similarly, acute and drastic spindle shortening was observed in most CENP-E inhibited cells after acute addition of the Aurora A inhibitor MLN8237 (125 nM), as expected from previous studies (Ye et al., 2015). Acute inhibition of PLK1 by BI 2536 (100 nM) induced a fast block of spindle elongation and cytokinetic invasion in cells after the onset of anaphase observed only after CENP-E washout, as expected from previous reports (Petronczki et al., 2007).

Regarding cells imaged by confocal microscopy after the chronic inhibition of CENP-E by GSK-923295 (80 nM), all pseudo-metaphase spindles chosen for imaging were phenotypically similar between each other and between conditions where CENP-E was depleted or reactivated after washout of the CENP-E inhibitor: 1) in all cells few chromosomes were localized close to one of the spindle poles, called polar chromosomes, and their numbers ranged from 2-16 per cell; 2) occasionally in some cells few chromosomes were localized already in between spindle pole and equator; and 3) in all cells most chromosomes were already aligned and tightly packed at the metaphase plate. This type of chromosome arrangement was expected from previously published data that reported that only 10-30% of chromosomes upon NEBD require CENP-E-mediated alignment (Barisic et al., 2014). Likewise, under all conditions where CENP-E was perturbed and cells imaged by confocal microscopy during pseudo-metaphase, the overall displacement of spindle poles from each other was negligible (data not shown), consistent with cells being in a pseudo-metaphase state where there is no net change in spindle length. For LLSM-based assay, no inclusion criteria for imaging were used as the cells were non-synchronized and entered mitosis stochastically. Only randomly selected cells that entered mitosis and subsequently entered anaphase during imaging time were used for kinetochore and centrosome tracking analysis.

Immunofluorescence

All cells were fixed for 2 minutes with ice-cold methanol, except for those used in STED microscopy, which are described below. After fixation, cells were washed 3 times for 5 min with 1 ml of PBS and permeabilized with 0.5% Triton-X-100 solution in water for 30 min at room temperature. To block unspecific binding, cells were incubated in 1 ml of blocking buffer (2% bovine serum albumin, BSA) for 2 h at room temperature. The cells were then washed 3 times for 5 min with 1 ml of PBS and incubated with 500 µl of primary antibody solution overnight at 4°C. Antibody incubation was performed using a blocking solution composed of 0.1% Triton, 1% BSA in PBS.

Following primary antibodies were used: rabbit monoclonal Anti-NDC80 (HPA066330-100uL, Sigma-Aldrich, diluted 1:250), mouse monoclonal anti-KIFC1 (M-6, sc-100947, Santa Cruz, diluted 1:500), rabbit polyclonal anti-Kif18a (A301-080A, Bethyl Laboratories, diluted 1:500), mouse monoclonal anti-BubR1 (MAB3612, EMD Milipore, diluted 1:500), rabbit anti-Kif4A (A301-074A, Bethyl Laboratories, diluted 1:500), rabbit anti-SPINDLY/CCD98 (A301-354A,

Bethyl Laboratories, diluted 1:500) and mouse monoclonal anti-KID (B-9, sc-390640, Santa Cruz, diluted 1:500).

After primary antibody, cells were washed in PBS and then incubated in 500 µL of secondary antibody solution for 1 h at room temperature. Following secondary antibodies were used: Donkey anti-rabbit IgG Alexa Fluor 594 (ab150064, Abcam, diluted 1:1000) for all rabbit antibodies, Donkey anti-mouse IgG Alexa Fluor 594 (ab150108, Abcam, diluted, 1:1000) for all mouse antibodies except anti-KID which was conjugated with Donkey anti-mouse IgG Alexa Fluor 647 (ab150107, Abcam, diluted 1:1000). Finally, cells were washed with 1 ml of PBS, 3 times for 10 min. Cells were imaged either immediately following the imaging or were kept at 4°C before imaging for a maximum period of one week.

To visualize alpha-tubulin in STED resolution in the RPE-1 CENP-A-GFP centrin1-GFP cell line, the ice-cold methanol protocol was avoided because it destroyed the unstable fraction of microtubules (Ponjavić et al., 2021). Cells were washed with cell extraction buffer (CEB) and fixed with 3.2% paraformaldehyde (PFA) and 0.1% glutaraldehyde (GA) in PEM buffer (0.1 M PIPES, 0.001 M MgCl2 × 6 H2O, 0.001 M EGTA, 0.5% Triton-X-100) for 10 min at room temperature. After fixation with PFA and GA, for quenching, cells were incubated in 1 ml of freshly prepared 0.1% borohydride in PBS for 7 min and then in 1 mL of 100 mM NH_4Cl and 100 mM glycine in PBS for 10 min at room temperature. To block nonspecific binding of antibodies, cells were incubated in 500 µL blocking/permeabilization buffer (2% normal goat serum and 0.5% Triton-X-100 in water) for 2 h at room temperature. Cells were then incubated in 500 µL of primary antibody solution containing rat anti-alpha-tubulin YL1/2 (MA1-80017, Invitrogen, CA, SAD, diluted 1:500) overnight at 4 °C. After incubation with a primary antibody, cells were washed 3 times for 10 min with 1 ml of PBS and then incubated with 500 µl of secondary antibody containing donkey anti-rat IgG Alexa Fluor 594 (ab150156, Abcam, diluted 1:300) for 2 h at room temperature, followed by wash with 1 ml of PBS 3 times for 10 min.

Imaging

Opterra I multipoint scanning confocal microscope system (Bruker Nano Surfaces, Middleton, WI, USA) was mainly used for live-cell imaging of hTERT-RPE1 cells expressing CENP-A-GFP and Centrin1-GFP, in cells depleted of CENP-E by siRNAs and in cells with inhibited CENP-E by CENP-E inhibitor, in the assay we termed a confocal-based imaging assay. The system was mounted on a Nikon Ti-E inverted microscope equipped with a Nikon CFI Plan Apo VC 100x/1.4 numerical aperture oil objective (Nikon, Tokyo, Japan). The system was controlled with Prairie View Imaging Software (Bruker). During imaging, cells were kept at 37 ° C and at 5% CO_2 in the Okolab cage incubator (Okolab, Pozzuoli, NA, Italy). The laser power was set to 10% for the 488nm excitation laser. For optimal resolution and signal-to-noise ratio, a 60 µm pinhole aperture was used and the xy-pixel size was set to 83 nm. For excitation of GFP, a 488-nm diode laser line was used. The excitation light was separated from the emitted fluorescence using the Opterra dichroic and Barrier 488 eGFP filter set (Chroma, USA). Images were acquired with an Evolve 512 Delta Electron Multiplying Charge Coupled Device (EMCCD) camera (Photometrics, Tucson, AZ, USA) using a 150-ms exposure time and with a camera readout mode of 20 MHz. 30-60 z-stacks encompassing all focal planes with visible green signal were acquired with 0.5 µm spacing

to cover the entire spindle area in depth with unidirectional xyz scan mode and with the “fast acquisition” option enabled in software. Images of six different cells were taken simultaneously every 30s-1 min. The total duration of the time-lapse movies was 30 min to 1 hour.

The STED confocal microscope system (Abberior Instruments) and the LSM800 laser scanning confocal system (Zeiss) were used for the remainder of the live-cell experiments we termed the confocal-based imaging assay and in hTERT-RPE1 cells expressing CENP-A-mCerulean and Mad2-mRuby after reactivation of CENP-E activity. STED microscopy was also used to image all fixed cells in super-resolution. STED microscopy was performed using an Expert Line easy3D STED microscope system (Abberior Instruments, Göttingen, Germany) with the 100 x/1.4NA UPLSAPO100x oil objective (Olympus, Tokio, Japan) and an avalanche photodiode detector (APD). The 488 nm line was used for excitation, with the addition of the 561 nm line for excitation and the 775 nm laser line for depletion during STED super-resolution imaging. The images were acquired using Imspector software. The xy pixel size for fixed cells was 20 nm and 10 focal planes were acquired with a 300 nm distance between the planes. For confocal live cell imaging of cells, the xy pixel size was 80 nm and 16 focal images were acquired, with 0.5 µm distance between the planes and 1 min time intervals between different frames. During imaging, live cells were kept at 37 ° C and at 5% CO_2 in the Okolab stage incubation chamber system (Okolab, Pozzuoli, NA, Italy).

LSM 800 confocal laser scanning microscope system (Zeiss) was used for the rest of live-cell confocal-based imaging in hTERT-RPE1 cells expressing CENP-A-GFP and centrin1-GFP with the following parameters: sampling in xy, 0.27 µm; z step size, 0.5 µm; total number of slices, 32; pinhole, 48.9 µm; unidirectional scan speed, 10; averaging, 2; 63x Oil DIC f/ELYRA objective (1.4 NA), 488 nm laser line (0.1% power), and detection ranges of 410–558 nm. Images were acquired using ZEN 2.6 (blue edition; Zeiss). Six cells in volumes of 15 µm were imaged sequentially every 1 minute at different positions determined right after the addition of a drug. During imaging, cells were incubated at 37 °C and 5% CO_2 using a Pecon stage incubation chamber system (Pecon, Heating Insert P S1, #130-800 005). The system was also used for imaging of all other fixed cells that were not imaged by STED microscopy, on multiples positions and at the confocal lateral resolution.

The Lattice Lightsheet 7 microscope system (Zeiss) was used for live cell imaging of hTERT-RPE1 cells expressing CENP-A-GFP and Centrin1-GFP and U2OS cells expressing CENP-A-GFP after reactivation of CENP-E activity, in cells depleted of CENP-E by siRNAs and in cells with inhibited CENP-E by CENP-E inhibitor, in assay we called LLSM-based imaging assay. The system was equipped with an illumination objective lens 13.3×/0.4 (at a 30° angle to cover the glass) with a static phase element and a detection objective lens 44.83×/1.0 (at a 60° angle to cover the glass) with an Alvarez manipulator. Images were acquired using ZEN 2.6 (blue edition; Zeiss). The automatic immersion of water was applied from the motorized dispenser at an interval of 20 or 30 minutes. Right after sample mounting, four steps of the 'create immersion' auto immersion option were applied. The sample was illuminated with a 488-nm diode laser (power output 10 Mw) with laser power set to 1-2%. The detection module consisted of a Hamamatsu ORCA-Fusion sCMOS camera with exposure time set to 15-20 ms. The LBF 405/488/561/642 emission filter

was used. During imaging, cells were kept at 37 °C and at 5% CO2 in a Zeiss stage incubation chamber system (Zeiss). The width of the imaging area in the x dimension was set from 1 to 1.5 mm.

Tracking of centrosomes and kinetochores

The spatial x and y coordinates of the kinetochore pairs were extracted in each time frame using the Low Light Tracking Tool (v.0.10), an ImageJ plugin based on the Nested Maximum Likelihood Algorithm, as previously described (Vukušić et al., 2021). Tracking of polar kinetochores in the x and y planes was performed on the maximum intensity projections of all acquired z planes. Some kinetochore pairs could not be successfully tracked in all frames, mainly owing to cell and spindle movements in the z-direction over time. Spindle poles were manually tracked with points placed between the center of the two centrioles or centriole in centrinone treated cells. Kinetochore pairs that were aligned at the start of the imaging in a confocal-based imaging assay were also manually tracked in two dimensions. Quantitative analysis of all parameters was performed using custom-made MATLAB scripts (MatlabR2021a 9.10.0) scripts.

Due to the inability to reliably track polar kinetochores across all time frames due to neighboring kinetochores, tracking of polar kinetochores routinely commenced a few frames before the kinetochore pair began moving towards the equatorial plane. In the CENP-E reactivation assay, kinetochores were tracked from the onset of imaging until the successful identification of the same kinetochore pair, which occurred when the kinetochore pair was lost in the imaging plane, among other kinetochores, or when the imaging session ended, whichever came first. Aligned kinetochore pairs were tracked in the confocal-based assay using the same protocol.

Quantification of mean Mad2 intensity of kinetochore pairs

The fluorescence intensity signal of each kinetochore in both CENP-A and Mad2 was measured by using the "*Oval selection*" tool in ImageJ with the size and position defined by the borders of the CENP-A signal of each kinetochore in the sum intensity projection of all acquired z-planes. The background fluorescence intensity measured in the cytoplasm was subtracted from the obtained values, and the calculated integrated intensity value was divided by the number of z-stacks used to generate the sum projection of each cell. The obtained mean intensity value subtracted for background for each kinetochore was normalized to the intensity of the CENP-A signal.

Quantification of mean signal intensities of proteins after RNAi interreference

The fluorescence intensity signals were measured in triplicate samples for targeting and non-targeting groups for each siRNA treatment. Each siRNA targeting and non-targeting triplicates were imaged by the same protocol. All proteins were measured in mitotic cells at their respective locations during mitosis by using the "*Polygon selection tool*", as established by many previous studies: kinetochores and chromosomes defined by the DAPI or CENP-A area on sum projection for CENP-E, Spindly, BubR1, and on single planes for Hec1 defined by the CENP-A signal; entire spindle region defined by extent of centrin-1 and CENP-A signals on sum projections for Kif4a, Kif18a, and HSET; and chromosomes defined by DAPI signal on sum projections for Kid.

Quantification of polar kinetochore pairs

Polar kinetochores in all experiments were defined as kinetochore pairs that are closer to one of the spindle poles than to the equatorial plane. In confocal-based experiments polar chromosomes were defined from the onset of imaging. The number of polar kinetochore pairs in cells that were imaged from the onset of mitosis, mainly related to LLSM-based experiments, was quantified 12 minutes from the onset of mitosis and then every 6 minutes until the onset of anaphase or until the end of the imaging on maximum intensity projections of all acquired z planes.

To calculate the distance between kinetochores in fixed samples, two points were placed at the center of the signal in each pair of kinetochores using a 'Point tool' in ImageJ. Congression velocity was calculated for each pair of kinetochores in the last 6 minutes before the center of the pair of kinetochores surpassed 2 μm from the equatorial plane measured as the nearest distance from a center of a pair to a plane. These times represent the fast kinetochore movement towards the plate. Aligned kinetochore pair was defined as every pair that was found 3 μm from the equatorial plane at any given time. The equatorial or metaphase plane was defined in each time frame as the line perpendicular to the line connecting the centrosomes at their midpoint. The angle between the kinetochore pairs and the main spindle axis was defined as an angle between a line connecting two centrosomes and a line connecting the center of the kinetochore pair and a spindle pole nearest to the respective pair.

In images acquired using STED microscopy, lateral attachments were defined as those in which the kinetochore did not form visible attachments with microtubules that terminate at the kinetochore, defined by the CENP-A signal; end-on attachments were defined as those in which the kinetochore formed visible attachments with microtubules that terminated at the kinetochore, defined by the CENP-A signal, with no visible microtubule signal just below or above the kinetochore. When scoring successful alignment of polar chromosomes, alignment was considered successful if a chromosome, initially polar at the beginning of imaging, moved to within 2 μm of the equatorial plane after 30 minutes. The 30-minute period was chosen because it represents the minimum imaging time used for the confocal-based microscopy assay, and it covers the majority of the imaged cells.

The alignment categories were defined as follows: "No metaphase plate" indicated that no metaphase plate is formed. "High misalignment" indicated a metaphase plate is formed, but more than 5 chromosomes are outside the plate. "Low misalignment" indicated a situation where a metaphase plate is formed, with fewer than 5 chromosomes outside the plate. Finally, "Tight metaphase plate" signified the formation of a tight metaphase plate with no chromosome misalignment. "Maximum spread of chromosomes" was measured on maximum intensity projections as the nearest distance between centers of two most separated kinetochore pairs.

Image processing and statistical analysis

Image processing was performed in ImageJ (National Institutes of Health, Bethesda, MD, USA). Quantification and statistical analysis were performed in MatLab. The figures were assembled in Adobe Illustrator CS6 (Adobe Systems, Mountain View, CA, USA). Raw images were used for quantification. The images of spindles were rotated in every frame to fit the long axis of the spindle

to be parallel with the central long axis of the box in ImageJ and the spindle short axis to be parallel with the central short axis of the designated box in ImageJ. The designated box sizes were cut to the same dimensions for all panels in the figures where the same experimental setups were used across the treatments. When comparing different treatments in channels in which the same protein was labeled, the minimum and maximum intensity of that channel was set to the values in the control treatment. When indicated, the smoothing of the images was performed using the "Gaussian blur" function in ImageJ (s=0.5-1.0). Colour-coded maximum intensity projections of the z-stacks were done using the "*Temporal colour code*" tool in Fiji by applying “16-color” or “Spectrum” lookup-table (LUT) or other LUT as indicated. For the generation of univariate scatter plots, the open Matlab extension “UnivarScatter” was used.

Data are given as mean ± standard deviation (s.t.d.), unless otherwise stated. The mean line was plotted to encompass a minimum of 60% of the data points for each treatment. Other dispersion measures used are defined in their respective figure captions or in Figure 1 and Appendix Figure S1 if the same measures are used across all figures. The exact values of n are given in the respective figure captions, where n represents the number of cells or the number of tracked kinetochore pairs, as defined for each n in the figure captions or tables. The number of independent biological replicates is also given in the figure captions. An independent experiment for acute drug treatments was defined by the separate addition of a drug to a population of cells in a dish. The number of cells imaged simultaneously ranged from 1 to 7, depending on the specific microscopy system used. The p values when comparing multiple classes were obtained using the one-way ANOVA test followed by Tukey's Honest Significant Difference (HSD) test (significance level was 5%). $p < 0.05$ was considered statistically significant, very significant if $0.001 < p < 0.01$ and extremely significant if $p < 0.001$. Values of all significant differences are given with the degree of significance indicated ($*0.01 < p < 0.05$, $**0.001 < p < 0.01$, $***p < 0.001$, $**** < 0.0001$). For the linear regression correlation measure between two parameters, the nonparametric Spearman correlation coefficient, termed rs, was used where $p<0.001$, calculated using the 'corr' function in Matlab (Statistics Toolbox R14). No statistical methods were used to predetermine the sample size. The experiments were not randomized and, except where stated, the investigators were not blinded to allocation during experiments and outcome evaluation.

DATA AVAILABILITY

This study includes no data deposited in external repositories.

DISCLOSURE AND COMPETING INTERESTS STATEMENT

The authors declare no competing interests.

REFERENCES

Ali, A., and P.T. Stukenberg. 2023. Aurora kinases: Generators of spatial control during mitosis. *Front. Cell Dev. Biol.* 11:265. doi:10.3389/FCELL.2023.1139367/BIBTEX.

Auckland, P., and A.D. McAinsh. 2015. Building an integrated model of chromosome congression. *J. Cell Sci.* 128:3363–3374. doi:10.1242/JCS.169367.

Bancroft, J., P. Auckland, C.P. Samora, and A.D. McAinsh. 2015. Chromosome congression is promoted by CENP-Q- and CENP-Edependent pathways. *J. Cell Sci.* 128:171–184. doi:10.1242/JCS.163659/-/DC1.

Barisic, M., P. Aguiar, S. Geley, and H. Maiato. 2014. Kinetochore motors drive congression of peripheral polar chromosomes by overcoming random arm-ejection forces. *Nat. Cell Biol.* 16:1249–1256. doi:10.1038/NCB3060.

Barisic, M., and H. Maiato. 2015. Dynein prevents erroneous kinetochore-microtubule attachments in mitosis. *Cell Cycle*. 14:3356. doi:10.1080/15384101.2015.1089369.

Barisic, M., and G. Rajendraprasad. 2021. Mitotic poleward flux: Finding balance between microtubule dynamics and sliding. *Bioessays*. 43. doi:10.1002/BIES.202100079.

Barisic, M., R. Silva E Sousa, S.K. Tripathy, M.M. Magiera, A. V. Zaytsev, A.L. Pereira, C. Janke, E.L. Grishchuk, and H. Maiato. 2015. Microtubule detyrosination guides chromosomes during mitosis. *Science (80-.).* 348:799–803. doi:10.1126/SCIENCE.AAA5175.

Barisic, M., B. Sohm, P. Mikolcevic, C. Wandke, V. Rauch, T. Ringer, M. Hess, G. Bonn, and S. Geley. 2010. Spindly/CCDC99 is required for efficient chromosome congression and mitotic checkpoint regulation. *Mol. Biol. Cell*. 21:1968–1981. doi:10.1091/MBC.E09-04-0356/ASSET/IMAGES/LARGE/ZMK0121094770007.JPEG.

Broad, A.J., K.F. DeLuca, and J.G. DeLuca. 2020. Aurora B kinase is recruited to multiple discrete kinetochore and centromere regions in human cells. *J. Cell Biol.* 219. doi:10.1083/JCB.201905144.

Cai, S., C.B. O'Connell, A. Khodjakov, and C.E. Walczak. 2009. Chromosome congression in the absence of kinetochore fibres. *Nat. Cell Biol.* 11:832–838. doi:10.1038/NCB1890.

Cane, S., A.A. Ye, S.J. Luks-Morgan, and T.J. Maresca. 2013. Elevated polar ejection forces stabilize kinetochore-microtubule attachments. *J. Cell Biol.* 200:203–218. doi:10.1083/JCB.201211119.

Cheerambathur, D.K., R. Gassmann, B. Cook, K. Oegema, and A. Desai. 2013. Crosstalk between microtubule attachment complexes ensures accurate chromosome segregation. *Science (80-.).* 342:1239–1242. doi:10.1126/SCIENCE.1246232/SUPPL_FILE/CHEERAMBATHUR.SM.PDF.

Chen, R.H., J.C. Waters, E.D. Salmon, and A.W. Murray. 1996. Association of spindle assembly checkpoint component XMAD2 with unattached kinetochores. *Science (80-.).* 274:242–246. doi:10.1126/SCIENCE.274.5285.242.

Cmentowski, V., G. Ciossani, E. d'Amico, S. Wohlgemuth, M. Owa, B. Dynlacht, and A. Musacchio. 2023. RZZ-Spindly and CENP-E form an integrated platform to recruit dynein to the kinetochore corona. *EMBO J.* 42. doi:10.15252/EMBJ.2023114838.

Collin, P., O. Nashchekina, R. Walker, and J. Pines. 2013. The spindle assembly checkpoint works like a rheostat rather than a toggle switch. *Nat. Cell Biol.* 15:1378–1385. doi:10.1038/ncb2855.

Cooke, C.A., B. Schaar, T.J. Yen, and W.C. Earnshaw. 1997. Localization of CENP-E in the fibrous corona and outer plate of mammalian kinetochores from prometaphase through anaphase. *Chromosoma*. 106:446–455. doi:10.1007/S004120050266.

Dai, J., S. Sultan, S.S. Taylor, and J.M.G. Higgins. 2005. The kinase haspin is required for mitotic histone H3 Thr 3 phosphorylation and normal metaphase chromosome alignment. *Genes Dev.* 19:472–488. doi:10.1101/GAD.1267105.

DeLuca, K.F., S.M.A. Lens, and J.G. DeLuca. 2011. Temporal changes in Hec1 phosphorylation control kinetochore–microtubule attachment stability during mitosis. *J. Cell Sci.* 124:622–634. doi:10.1242/JCS.072629.

Ditchfield, C., V.L. Johnson, A. Tighe, R. Ellston, C. Haworth, T. Johnson, A. Mortlock, N. Keen, and S.S. Taylor. 2003. Aurora B couples chromosome alignment with anaphase by targeting BubR1, Mad2, and Cenp-E to kinetochores. *J. Cell Biol.* 161:267–280. doi:10.1083/JCB.200208091.

Drpic, D., A.J. Pereira, M. Barisic, T.J. Maresca, and H. Maiato. 2015. Polar Ejection Forces Promote the Conversion from Lateral to End-on Kinetochore-Microtubule Attachments on Mono-oriented Chromosomes. *Cell Rep.* 13:460–468. doi:10.1016/J.CELREP.2015.08.008.

Ehlén, Å., C. Martin, S. Miron, M. Julien, F.X. Theillet, V. Ropars, G. Sessa, R. Beaurepere, V. Boucherit, P. Duchambon, A. El Marjou, S. Zinn-Justin, and A. Carreira. 2020. Proper chromosome alignment depends on BRCA2 phosphorylation by PLK1. *Nat. Commun. 2020 111*. 11:1–21. doi:10.1038/s41467-020-15689-9.

Eibes, S., G. Rajendraprasad, C. Guasch-Boldu, M. Kubat, Y. Steblyanko, and M. Barisic. 2023. CENP-E activation by Aurora A and B controls kinetochore fibrous corona disassembly. *Nat. Commun. 2023 141*. 14:1–14. doi:10.1038/s41467-023-41091-2.

Etemad, B., T.E.F. Kuijt, and G.J.P.L. Kops. 2015. Kinetochore–microtubule attachment is sufficient to satisfy the human spindle assembly checkpoint. *Nat. Commun. 2015 61*. 6:1–8. doi:10.1038/ncomms9987.

Famulski, J.K., and G.K. Chan. 2007. Aurora B kinase-dependent recruitment of hZW10 and hROD to tensionless kinetochores. *Curr. Biol.* 17:2143–2149. doi:10.1016/J.CUB.2007.11.037.

Fiorentini, C., P. Matarrese, A. Fattorossi, and G. Donelli. 1996. Okadaic acid induces changes in the organization of F-actin in intestinal cells. *Toxicon*. 34:937–945. doi:10.1016/0041-0101(96)00025-6.

Firestone, A.J., J.S. Weinger, M. Maldonado, K. Barlan, L.D. Langston, M. O'Donnell, V.I. Gelfand, T.M. Kapoor, and J.K. Chen. 2012. Small-molecule inhibitors of the AAA+

ATPase motor cytoplasmic dynein. *Nature*. 484:125–129. doi:10.1038/NATURE10936.

Gassmann, R. 2023. Dynein at the kinetochore. *J. Cell Sci.* 136. doi:10.1242/JCS.220269/291809.

Gassmann, R., A.J. Holland, D. Varma, X. Wan, F. Çivril, D.W. Cleveland, K. Oegema, E.D. Salmon, and A. Desai. 2010. Removal of Spindly from microtubule-attached kinetochores controls spindle checkpoint silencing in human cells. *Genes Dev.* 24:957–971. doi:10.1101/GAD.1886810.

Gomes, A.M., B. Orr, M. Novais-Cruz, F. De Sousa, J. Macário-Monteiro, C. Lemos, C. Ferrás, and H. Maiato. 2022. Micronuclei from misaligned chromosomes that satisfy the spindle assembly checkpoint in cancer cells. *Curr. Biol.* 32:4240-4254.e5. doi:10.1016/J.CUB.2022.08.026.

Gudimchuk, N., B. Vitre, Y. Kim, A. Kiyatkin, D.W. Cleveland, F.I. Ataullakhanov, and E.L. Grishchuk. 2013. Kinetochore kinesin CENP-E is a processive bi-directional tracker of dynamic microtubule tips. *Nat. Cell Biol.* 15:1079–1088. doi:10.1038/NCB2831.

Hadders, M.A., S. Hindriksen, M.A. Truong, A.N. Mhaskar, J. Pepijn Wopken, M.J.M. Vromans, and S.M.A. Lens. 2020. Untangling the contribution of Haspin and Bub1 to Aurora B function during mitosis. *J. Cell Biol.* 219. doi:10.1083/JCB.201907087.

Hengeveld, R.C.C., M.J.M. Vromans, M. Vleugel, M.A. Hadders, and S.M.A. Lens. 2017. Inner centromere localization of the CPC maintains centromere cohesion and allows mitotic checkpoint silencing. *Nat. Commun.* 8. doi:10.1038/ncomms15542.

Hindriksen, S., S.M.A. Lens, and M.A. Hadders. 2017. The ins and outs of Aurora B inner centromere localization. *Front. Cell Dev. Biol.* 5:112. doi:10.3389/FCELL.2017.00112/BIBTEX.

Huang, Y., L. Lin, X. Liu, S. Ye, P.Y. Yao, W. Wang, F. Yang, X. Gao, J. Li, Y. Zhang, J. Zhang, Z. Yang, X. Liu, Z. Yang, J. Zang, M. Teng, Z. Wang, K. Ruan, X. Ding, L. Li, D.W. Cleveland, R. Zhang, and X. Yao. 2019. BubR1 phosphorylates CENP-E as a switch enabling the transition from lateral association to end-on capture of spindle microtubules. *Cell Res.* 29:562. doi:10.1038/S41422-019-0178-Z.

Iemura, K., and K. Tanaka. 2015. Chromokinesin Kid and kinetochore kinesin CENP-E differentially support chromosome congression without end-on attachment to microtubules. *Nat. Commun.* 6. doi:10.1038/NCOMMS7447.

Itoh, G., M. Ikeda, K. Iemura, M.A. Amin, S. Kuriyama, M. Tanaka, N. Mizuno, H. Osakada, T. Haraguchi, and K. Tanaka. 2018. Lateral attachment of kinetochores to microtubules is enriched in prometaphase rosette and facilitates chromosome alignment and bi-orientation establishment. *Sci. Rep.* 8. doi:10.1038/S41598-018-22164-5.

Kajtez, J., A. Solomatina, M. Novak, B. Polak, K. Vukušić, J. Rüdiger, G. Cojoc, A. Milas, I. Šumanovac Šestak, P. Risteski, F. Tavano, A.H. Klemm, E. Roscioli, J. Welburn, D. Cimini, M. Glunčić, N. Pavin, and I.M. Tolić. 2016. Overlap microtubules link sister k-fibres and balance the forces on bi-oriented kinetochores. *Nat. Commun.* 7. doi:10.1038/NCOMMS10298.

Kapoor, T.M., M.A. Lampson, P. Hergert, L. Cameron, D. Cimini, E.D. Salmon, B.F. McEwen, and A. Khodjakov. 2006. Chromosomes can congress to the metaphase plate before biorientation. *Science (80-.).* 311:388–391. doi:10.1126/SCIENCE.1122142.

Kapoor, T.M., T.U. Mayer, M.L. Coughlin, and T.J. Mitchison. 2000. Probing spindle assembly mechanisms with monastrol, a small molecule inhibitor of the mitotic kinesin, Eg5. *J. Cell Biol.* 150:975–988. doi:10.1083/JCB.150.5.975.

Kawashima, S.A., T. Tsukahara, M. Langegger, S. Hauf, T.S. Kitajima, and Y. Watanabe. 2007. Shugoshin enables tension-generating attachment of kinetochores by loading Aurora to centromeres. *Genes Dev.* 21:420–435. doi:10.1101/GAD.1497307.

Kim, Y., J.E. Heuser, C.M. Waterman, and D.W. Cleveland. 2008. CENP-E combines a slow, processive motor and a flexible coiled coil to produce an essential motile kinetochore tether. *J. Cell Biol.* 181:411–419. doi:10.1083/JCB.200802189.

Kim, Y., A.J. Holland, W. Lan, and D.W. Cleveland. 2010. Aurora kinases and protein phosphatase 1 mediate chromosome congression through regulation of CENP-E. *Cell*. 142:444–455. doi:10.1016/J.CELL.2010.06.039.

Klaasen, S.J., M.A. Truong, R.H. van Jaarsveld, I. Koprivec, V. Štimac, S.G. de Vries, P. Risteski, S. Kodba, K. Vukušić, K.L. de Luca, J.F. Marques, E.M. Gerrits, B. Bakker, F. Foijer, J. Kind, I.M. Tolić, S.M.A. Lens, and G.J.P.L. Kops. 2022. Nuclear chromosome locations dictate segregation error frequencies. *Nature*. 607:604–609. doi:10.1038/S41586-022-04938-0.

Kops, G.J.P.L., and R. Gassmann. 2020. Crowning the Kinetochore: The Fibrous Corona in Chromosome Segregation. *Trends Cell Biol.* 30:653–667. doi:10.1016/J.TCB.2020.04.006.

Kruse, T., G. Zhang, M.S.Y. Larsen, T. Lischetti, W. Streicher, T.K. Nielsen, S.P. Bjørn, and J. Nilsson. 2013. Direct binding between BubR1 and B56-PP2A phosphatase complexes regulate mitotic progression. *J. Cell Sci.* 126:1086–1092. doi:10.1242/JCS.122481/263505/AM/DIRECT-BINDING-BETWEEN-BUBR1-AND-B56-PP2A.

Kuhn, J., and S. Dumont. 2017. Spindle assembly checkpoint satisfaction occurs via end-on but not lateral attachments under tension. *J. Cell Biol.* 216:1533–1542. doi:10.1083/JCB.201611104.

Lampson, M.A., and T.M. Kapoor. 2005. The human mitotic checkpoint protein BubR1 regulates chromosome-spindle attachments. *Nat. Cell Biol.* 7:93–98. doi:10.1038/NCB1208.

Lampson, M.A., K. Renduchitala, A. Khodjakov, and T.M. Kapoor. 2004. Correcting improper chromosome-spindle attachments during cell division. *Nat. Cell Biol.* 6:232–237. doi:10.1038/ncb1102.

Legal, T., D. Hayward, A. Gluszek-Kustusz, E.A. Blackburn, C. Spanos, J. Rappsilber, U. Gruneberg, and J.P.I. Welburn. 2020. The C-terminal helix of BubR1 is essential for CENP-E-dependent chromosome alignment. *J. Cell Sci.* 133. doi:10.1242/JCS.246025.

Lončarek, J., O. Kisurina-Evgenieva, T. Vinogradova, P. Hergert, S. La Terra, T.M. Kapoor, and A. Khodjakov. 2007. The centromere geometry essential for keeping mitosis error free is

controlled by spindle forces. *Nat. 2007 4507170*. 450:745–749. doi:10.1038/nature06344.

Magidson, V., C.B. O'Connell, J. Lončarek, R. Paul, A. Mogilner, and A. Khodjakov. 2011. The spatial arrangement of chromosomes during prometaphase facilitates spindle assembly. *Cell*. 146:555–567. doi:10.1016/J.CELL.2011.07.012.

Maia, A.F., T. Feijão, M.J.M. Vromans, C.E. Sunkel, and S.M.A. Lens. 2010. Aurora B kinase cooperates with CENP-E to promote timely anaphase onset. *Chromosoma*. 119:405–413. doi:10.1007/S00412-010-0265-X/FIGURES/8.

Maiato, H., A.M. Gomes, F. Sousa, and M. Barisic. 2017. Mechanisms of Chromosome Congression during Mitosis. *Biol. 2017, Vol. 6, Page 13*. 6:13. doi:10.3390/BIOLOGY6010013.

Mao, Y., A. Desai, and D.W. Cleveland. 2005. Microtubule capture by CENP-E silences BubR1-dependent mitotic checkpoint signaling. *J. Cell Biol.* 170:873–880. doi:10.1083/JCB.200505040.

Matković, J., S. Ghosh, M. Ćosić, S. Eibes, M. Barišić, N. Pavin, and I.M. Tolić. 2022. Kinetochore- and chromosome-driven transition of microtubules into bundles promotes spindle assembly. *Nat. Commun.* 13. doi:10.1038/S41467-022-34957-4.

McAinsh, A.D., and G.J.P.L. Kops. 2023. Principles and dynamics of spindle assembly checkpoint signalling. *Nat. Rev. Mol. Cell Biol.* 24:543–559. doi:10.1038/S41580-023-00593-Z.

McEwen, B.F., G.K.T. Chan, B. Zubrowski, M.S. Savoian, M.T. Sauer, and T.J. Yen. 2001. CENP-E is essential for reliable bioriented spindle attachment, but chromosome alignment can be achieved via redundant mechanisms in mammalian cells. *Mol. Biol. Cell*. 12:2776–2789. doi:10.1091/MBC.12.9.2776.

McEwen, B.F., A.B. Heagle, G.O. Cassels, K.F. Buttle, and C.L. Rieder. 1997. Kinetochore fiber maturation in PtK1 cells and its implications for the mechanisms of chromosome congression and anaphase onset. *J. Cell Biol.* 137:1567–1580. doi:10.1083/jcb.137.7.1567.

Petronczki, M., M. Glotzer, N. Kraut, and J.M. Peters. 2007. Polo-like kinase 1 triggers the initiation of cytokinesis in human cells by promoting recruitment of the RhoGEF Ect2 to the central spindle. *Dev. Cell*. 12:713–725. doi:10.1016/J.DEVCEL.2007.03.013.

Polak, B., P. Risteski, S. Lesjak, and I.M. Tolić. 2017. PRC 1-labeled microtubule bundles and kinetochore pairs show one-to-one association in metaphase . *EMBO Rep.* 18:217–230. doi:10.15252/EMBR.201642650.

Ponjavić, I., K. Vukušić, and I.M. Tolić. 2021. Expansion microscopy of the mitotic spindle. *Methods Cell Biol.* 161:247–274. doi:10.1016/BS.MCB.2020.04.014.

Renda, F., C. Miles, I. Tikhonenko, R. Fisher, L. Carlini, T.M. Kapoor, A. Mogilner, and A. Khodjakov. 2022. Non-centrosomal microtubules at kinetochores promote rapid chromosome biorientation during mitosis in human cells. *Curr. Biol.* doi:10.1016/J.CUB.2022.01.013.

Risteski, P., D. Božan, M. Jagrić, A. Bosilj, N. Pavin, and I.M. Tolić. 2022. Length-dependent

poleward flux of sister kinetochore fibers promotes chromosome alignment. *Cell Rep.* 40. doi:10.1016/J.CELREP.2022.111169.

Sacristan, C., M.U.D. Ahmad, J. Keller, J. Fermie, V. Groenewold, E. Tromer, A. Fish, R. Melero, J.M. Carazo, J. Klumperman, A. Musacchio, A. Perrakis, and G.J. Kops. 2018. Dynamic kinetochore size regulation promotes microtubule capture and chromosome biorientation in mitosis. *Nat. Cell Biol. 2018 207*. 20:800–810. doi:10.1038/s41556-018-0130-3.

Salimian, K.J., E.R. Ballister, E.M. Smoak, S. Wood, T. Panchenko, M.A. Lampson, and B.E. Black. 2011. Feedback control in sensing chromosome biorientation by the Aurora B kinase. *Curr. Biol.* 21:1158–1165. doi:10.1016/J.CUB.2011.06.015.

Santaguida, S., C. Vernieri, F. Villa, A. Ciliberto, and A. Musacchio. 2011. Evidence that Aurora B is implicated in spindle checkpoint signalling independently of error correction. *EMBO J.* 30:1508–1519. doi:10.1038/EMBOJ.2011.70.

Schaar, B.T., G.K.T. Chan, P. Maddox, E.D. Salmon, and T.J. Yen. 1997. CENP-E function at kinetochores is essential for chromosome alignment. *J. Cell Biol.* 139:1373–1382. doi:10.1083/JCB.139.6.1373.

Shrestha, R.L., D. Conti, N. Tamura, D. Braun, R.A. Ramalingam, K. Cieslinski, J. Ries, and V.M. Draviam. 2017. Aurora-B kinase pathway controls the lateral to end-on conversion of kinetochore-microtubule attachments in human cells. *Nat. Commun.* 8. doi:10.1038/S41467-017-00209-Z.

Shrestha, R.L., and V.M. Draviam. 2013. Lateral to end-on conversion of chromosome-microtubule attachment requires kinesins cenp-e and MCAK. *Curr. Biol.* 23:1514–1526. doi:10.1016/J.CUB.2013.06.040.

Sikirzhytski, V., F. Renda, I. Tikhonenko, V. Magidson, B.F. McEwen, and A. Khodjakov. 2018. Microtubules assemble near most kinetochores during early prometaphase in human cells. *J. Cell Biol.* 217:2647–2659. doi:10.1083/JCB.201710094.

Song, X., D. Conti, R.L. Shrestha, D. Braun, and V.M. Draviam. 2021. Counteraction between Astrin-PP1 and Cyclin-B-CDK1 pathways protects chromosome-microtubule attachments independent of biorientation. *Nat. Commun.* 12. doi:10.1038/S41467-021-27131-9.

Stumpff, J., G. von Dassow, M. Wagenbach, C. Asbury, and L. Wordeman. 2008. The Kinesin-8 Motor Kif18A Suppresses Kinetochore Movements to Control Mitotic Chromosome Alignment. *Dev. Cell*. 14:252–262. doi:10.1016/J.DEVCEL.2007.11.014.

Su, K.C., Z. Barry, N. Schweizer, H. Maiato, M. Bathe, and I.M.P. Cheeseman. 2016. A Regulatory Switch Alters Chromosome Motions at the Metaphase-to-Anaphase Transition. *Cell Rep.* 17:1728–1738. doi:10.1016/J.CELREP.2016.10.046.

Suijkerbuijk, S.J.E., T.J.P. van Dam, G.E. Karagöz, E. von Castelmur, N.C. Hubner, A.M.S. Duarte, M. Vleugel, A. Perrakis, S.G.D. Rüdiger, B. Snel, and G.J.P.L. Kops. 2012. The Vertebrate Mitotic Checkpoint Protein BUBR1 Is an Unusual Pseudokinase. *Dev. Cell*. 22:1321–1329. doi:10.1016/J.DEVCEL.2012.03.009.

Taveras, C., C. Liu, and Y. Mao. 2019. A tension-independent mechanism reduces Aurora B-

mediated phosphorylation upon microtubule capture by CENP-E at the kinetochore. *Cell Cycle*. 18:1349. doi:10.1080/15384101.2019.1617615.

Tovini, L., and S.E. McClelland. 2019. Impaired CENP-E Function Renders Large Chromosomes More Vulnerable to Congression Failure. *Biomol. 2019, Vol. 9, Page 44*. 9:44. doi:10.3390/BIOM9020044.

Tucker, J.B., S.C. Bonema, R. García-Varela, R.A. Denu, Y. Hu, S.M. McGregor, M.E. Burkard, and B.A. Weaver. 2023. Misaligned Chromosomes are a Major Source of Chromosomal Instability in Breast Cancer. *Cancer Res. Commun.* 3:54–65. doi:10.1158/2767-9764.CRC-22-0302.

Valdez, V.A., L. Neahring, S. Petry, and S. Dumont. 2023. Mechanisms underlying spindle assembly and robustness. *Nat. Rev. Mol. Cell Biol.* 24:523–542. doi:10.1038/S41580-023-00584-0.

Vukušić, K., I. Ponjavić, R. Buđa, P. Risteski, and I.M. Tolić. 2021. Microtubule-sliding modules based on kinesins EG5 and PRC1-dependent KIF4A drive human spindle elongation. *Dev. Cell*. 56:1253-1267.e10. doi:10.1016/J.DEVCEL.2021.04.005/ATTACHMENT/680C448C-DA20-433C-9F27-C90D96D86C9D/MMC1.PDF.

Vukušić, K., and I.M. Tolić. 2022. Polar Chromosomes-Challenges of a Risky Path. *Cells*. 11. doi:10.3390/CELLS11091531.

Vukušić, K., and I.M. Tolić. 2024. Kinetochore-centrosome feedback linking CENP-E and Aurora kinases regulates chromosome biorientation. *bioRxiv*

Walczak, C.E., S. Cai, and A. Khodjakov. 2010. Mechanisms of chromosome behaviour during mitosis. *Nat. Rev. Mol. Cell Biol.* 11:91–102. doi:10.1038/NRM2832.

Weaver, B.A.A., Z.Q. Bonday, F.R. Putkey, G.J.P.L. Kops, A.D. Silk, and D.W. Cleveland. 2003. Centromere-associated protein-E is essential for the mammalian mitotic checkpoint to prevent aneuploidy due to single chromosome loss. *J. Cell Biol.* 162:551–563. doi:10.1083/JCB.200303167.

Weber, J., T. Legal, A.P. Lezcano, A. Gluszek-Kustusz, C. Paterson, S. Eibes, M. Barisic, O.R. Davies, and J.P.I. Welburn. 2024. A conserved CENP-E region mediates BubR1-independent recruitment to the outer corona at mitotic onset. *Curr. Biol.* 34:1133-1141.e4. doi:10.1016/J.CUB.2024.01.042.

Wood, K.W., L. Lad, L. Luo, X. Qian, S.D. Knight, N. Nevins, K. Brejc, D. Sutton, A.G. Gilmartin, P.R. Chua, R. Desai, S.P. Schauer, D.E. McNulty, R.S. Annan, L.D. Belmont, C. Garcia, Y. Lee, M.A. Diamond, L.F. Faucette, M. Giardiniere, S.Y. Zhang, C.M. Sun, J.D. Vidal, S. Lichtsteiner, W.D. Cornwell, J.D. Greshock, R.F. Wooster, J.T. Finer, R.A. Copeland, P.S. Huang, D.J. Morgans, D. Dhanak, G. Bergnes, R. Sakowicz, and J.R. Jackson. 2010. Antitumor activity of an allosteric inhibitor of centromere-associated protein-E. *Proc. Natl. Acad. Sci. U. S. A.* 107:5839–5844. doi:10.1073/PNAS.0915068107.

Wu, J., A. Larreategui-Aparicio, M.L.A. Lambers, D.L. Bodor, S.J. Klaasen, E. Tollenaar, M. de Ruijter-Villani, and G.J.P.L. Kops. 2023. Microtubule nucleation from the fibrous corona

by LIC1-pericentrin promotes chromosome congression. *Curr. Biol.* 33. doi:10.1016/J.CUB.2023.01.010.

Yang, J., T. Ikezoe, C. Nishioka, T. Tasaka, A. Taniguchi, Y. Kuwayama, N. Komatsu, K. Bandobashi, K. Togitani, H.P. Koeffler, H. Taguchi, and A. Yokoyama. 2007. AZD1152, a novel and selective aurora B kinase inhibitor, induces growth arrest, apoptosis, and sensitization for tubulin depolymerizing agent or topoisomerase II inhibitor in human acute leukemia cells in vitro and in vivo. *Blood*. 110:2034–2040. doi:10.1182/BLOOD-2007-02-073700.

Yao, X., K.L. Anderson, and D.W. Cleveland. 1997. The microtubule-dependent motor centromere-associated protein E (CENP-E) is an integral component of kinetochore corona fibers that link centromeres to spindle microtubules. *J. Cell Biol.* 139:435–447. doi:10.1083/JCB.139.2.435.

Ye, A.A., J. Deretic, C.M. Hoel, A.W. Hinman, D. Cimini, J.P. Welburn, and T.J. Maresca. 2015. Aurora A Kinase Contributes to a Pole-Based Error Correction Pathway. *Curr. Biol.* 25:1842–1851. doi:10.1016/J.CUB.2015.06.021.

Yen, T.J., D.A. Compton, D. Wise, R.P. Zinkowski, B.R. Brinkley, W.C. Earnshaw, and D.W. Cleveland. 1991. CENP-E, a novel human centromere-associated protein required for progression from metaphase to anaphase. *EMBO J.* 10:1245–1254. doi:10.1002/J.1460-2075.1991.TB08066.X.

Yen, T.J., G. Li, B.T. Schaar, I. Szilak, and D.W. Cleveland. 1992. CENP-E is a putative kinetochore motor that accumulates just before mitosis. *Nature*. 359:536–539. doi:10.1038/359536A0.

Yu, K.W., N. Zhong, Y. Xiao, and Z.Y. She. 2019. Mechanisms of kinesin-7 CENP-E in kinetochore-microtubule capture and chromosome alignment during cell division. *Biol. cell*. 111:143–160. doi:10.1111/BOC.201800082.

SUPPLEMENTARY FIGURE LEGENDS

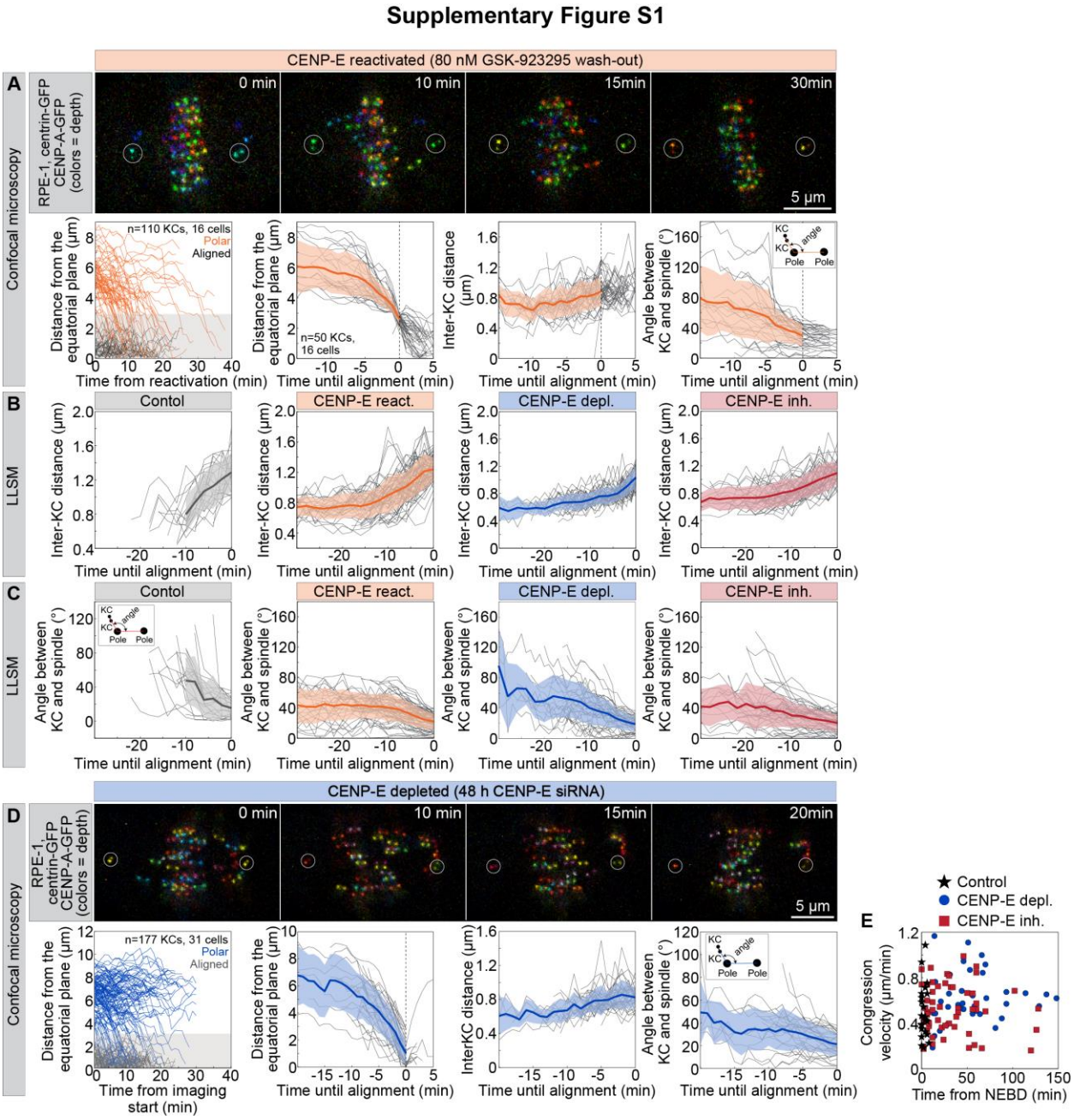

Figure S1. Chromosome movement during congression is similar in RPE-1 cells regardless of CENP-E activity and duration of mitosis, related to Figure 1. (A) Representative example of an RPE1 cell expressing CENP-A-GFP and centrin1-GFP in different frames as depicted after wash-out of the CENP-E inhibitor 80 nM GSK923295 and imaging by confocal microscopy. The image is a maximum projection color-coded by depth as specified by the color bar on Figure 1A (top). Distance from the equatorial plane of sister kinetochores for initially polar (orange lines) and aligned (black lines) kinetochore pairs in time from the washout of the CENP-E inhibitor, distance from the equatorial plane of sister kinetochores for initially polar kinetochore pairs,

distance between sister kinetochores (inter-KC), and angle between sister kinetochores and the main spindle axis, as depicted in a scheme in the top-left graph in time until alignment of the kinetochore pair across the indicated treatment. Thick lines represent means, and grey areas over means represent standard deviations (bottom). Centrioles are rounded by the white circle. (B) Distance between polar kinetochores (inter-KC) in time until alignment of the kinetochore pair across indicated treatments for cells imaged by lattice light sheet microscopy (LLSM). (C) Angle between polar kinetochores and the main spindle axis, as depicted in a scheme in the top-left graph in time until alignment of the kinetochore pair across indicated treatments for cells imaged by LLSM. (D) Representative example of an RPE1 cell expressing CENP-A-GFP and centrin1-GFP in different frames as depicted after depletion of CENP-E for 48h and imaged by confocal microscopy. The image is a maximum projection color-coded by depth as specified by the color bar on Figure 1A (top). Distance from the equatorial plane of sister kinetochores for initially polar (blue lines) and aligned (black lines) pairs in time from the washout of the CENP-E inhibitor, distance from the equatorial plane of sister kinetochores for initially polar kinetochore pairs, distance between sister kinetochores (inter-KC), and angle between sister kinetochores and the main spindle axis, as depicted in a scheme in the top-left graph in time until alignment of the kinetochore pair across the indicated treatment. Thick lines represent means, and grey areas over means represent standard deviations (bottom). (E) Congression velocity for polar kinetochore pairs during the last 6 minutes of chromosome congression versus time from nuclear envelope breakdown (NEBD) for treatments indicated in the legend on the left. Statistics: Tukey's HSD test. KC, kinetochore; depl., depleted; inh., inhibited; react., reactivated; NEBD, nuclear envelope breakdown.

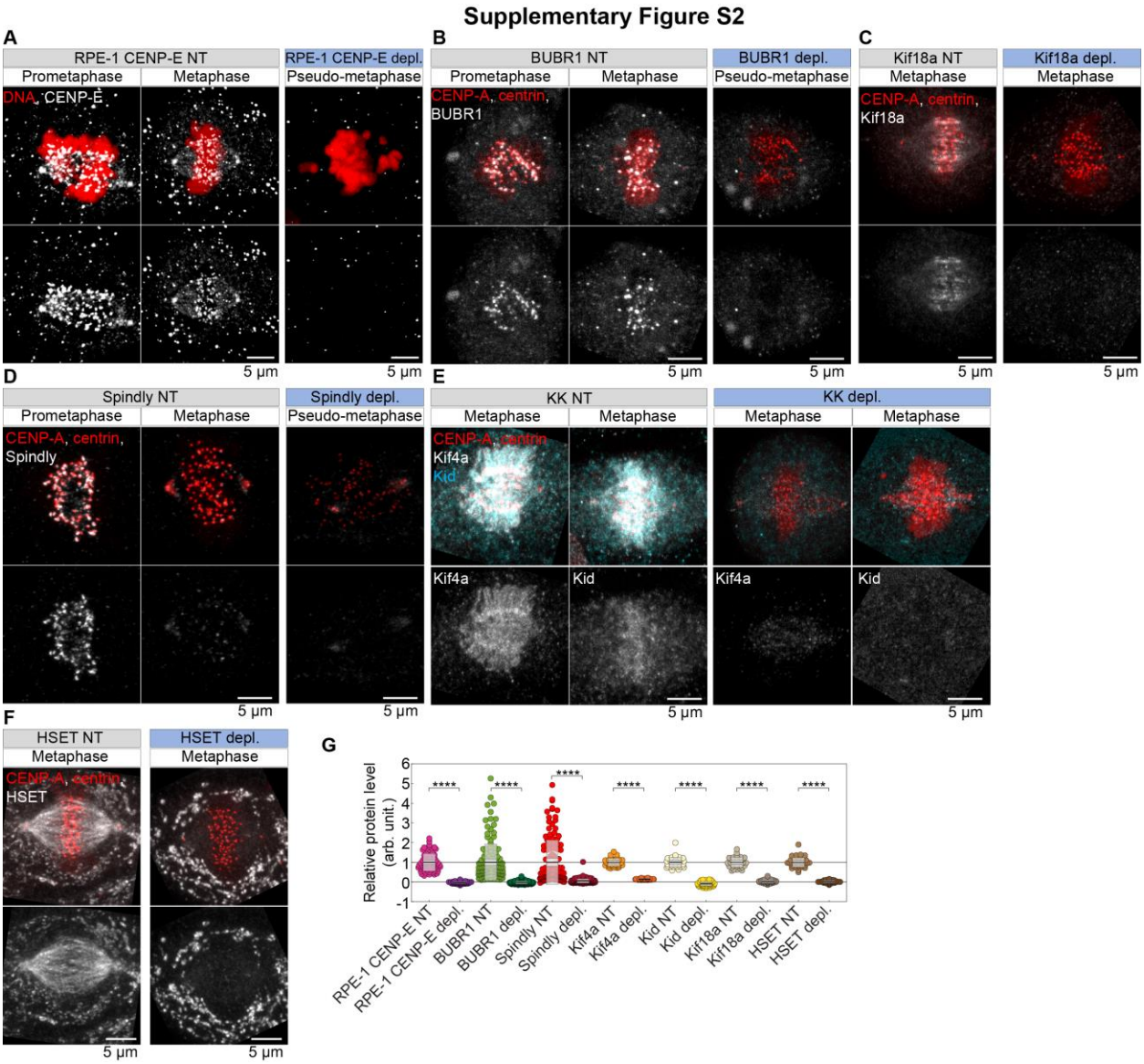

Figure S2. Immunofluorescence analysis of RNA interference efficiency for various targets, related to all figures. (A-F) Representative examples of RPE-1 cells after treatment with non-targeting (NT) small interfering RNAs (siRNAs) and immunofluorescence with antibodies targeting proteins depicted in gray, in different stages of mitosis as labeled (left) and after treatment with targeting siRNAs for different targets as indicated (right). RPE-1 cells were either wild-type (WT) and stained with DAPI (A, red) or expressed CENP-A-GFP and centrin-GFP (C-G, red). Top images represent maximum projections with merged channels, and bottom images represent only the channel in gray, representing the signal of the antibody targeting the protein that was targeted by the depicted siRNA. (G) Average protein level relative to the average of the non-targeting control group for depicted proteins. Numbers: 70, 66 cells (CENP-E); 137, 116, 121, 144 kinetochores from 14, 13, 15, 15 cells (BubR1 and Spindly); 36, 42, 35, 43, 34, 38, 42 and 36 cells (Kid to HSET), all in at least two independent experiments. depl., depletion. Statistics: Tukey's

HSD test. Symbols indicate: ****$P \leq 0.0001$. NT, non-targeting; depl., depleted; KK, Kid and Kif4a.

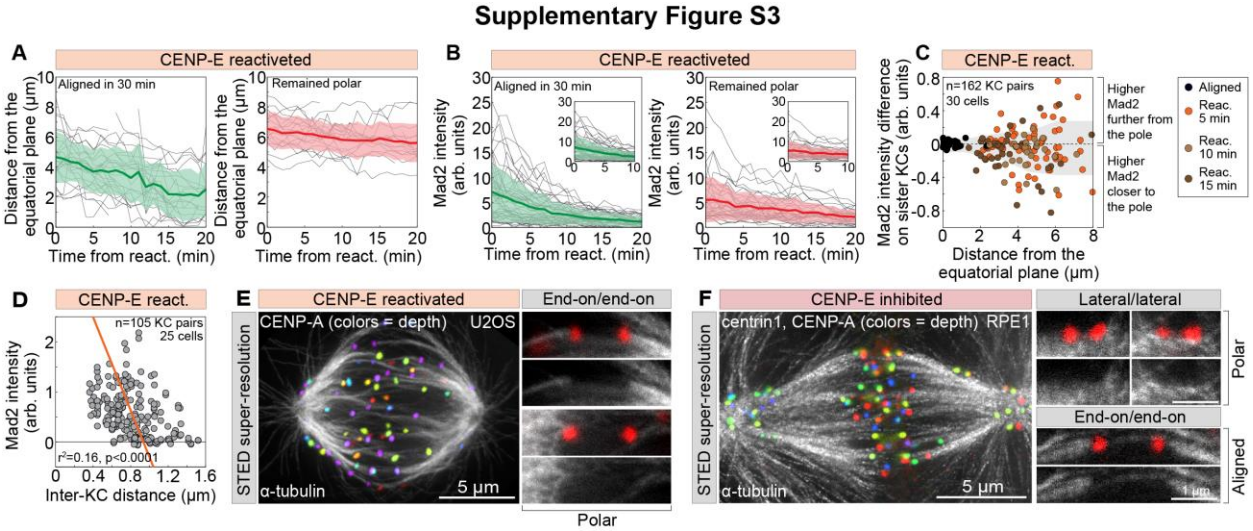

Figure S3. The Mad2 signal on polar kinetochores gradually decreases over time before the onset of chromosome movement, related to Figures 2 and 4. (A, B) Distance from the equatorial plane (A), and mean Mad2 signal intensity (B) of polar kinetochore pairs over time from the washout of the CENP-E inhibitor for kinetochore pairs that aligned in the 30-minute period (green, left parts) and pairs that did not align in the same period (red, right parts). (C) Distance of kinetochore pairs from the equatorial plane versus difference in Mad2 levels between two sister kinetochores based on proximity of each kinetochore in a pair to the nearest pole under conditions depicted on the right. (D) Interkinetochore (Inter-KC) distance of sister kinetochore pairs versus mean Mad2 signal intensity of sister kinetochore pairs with linear regression (line). (E, F) Representative examples of U2OS spindle 8 minutes after CENP-E reactivation (E) or RPE-1 spindle after CENP-E inhibition (F), immunostained for α-tubulin and imaged by stimulated emission depletion (STED) microscopy in cells expressing CENP-A-GFP (U2OS) or CENP-A-GFP and centrin1-GFP (RPE-1). Maximum intensity projection is color-coded by depth as specified by the color bar in Figure 1A (left). Insets of kinetochore pairs with microtubules from different attachment categories, as depicted, and schemes of microtubules (white) and kinetochores (red) of the respective insets (right). Statistics: Tukey's HSD test. Symbols indicate: n.s. $P > 0.05$, ****$P \leq 0.0001$.KC, kinetochore; inh., inhibited; reac., reactivated; arb., arbitrarily.

Supplementary Figure S4

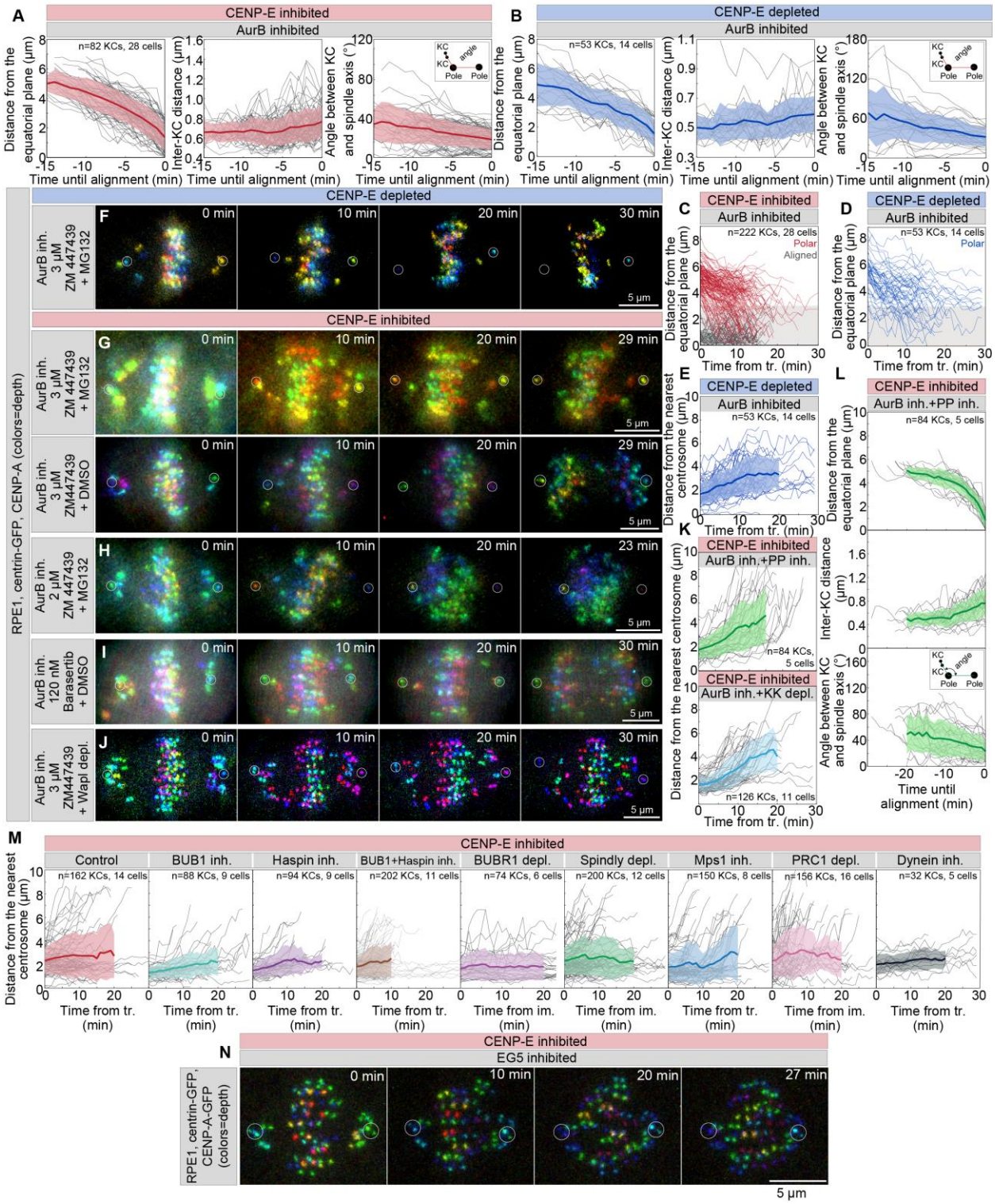

Figure S4. Chromosome congression in the absence of CENP-E is primarily limited by the activity of the outer-kinetochore pool of Aurora B, related to Figure 5. (A, B) Distance to the equatorial plane of polar kinetochore pairs (left), interkinetochore (inter-KC) distance (middle),

and angle between sister kinetochores and the main spindle axis as depicted in the scheme at the top (right) over time until alignment of kinetochore pairs after Aurora B acute inhibition by 3 µM ZM447439 in the CENP-E inhibited (A) or depleted (B) cells. Thick lines represent means, and grey areas around the means represent standard deviations. Centrioles are rounded by white circles. (C, D) Distance to the equatorial plane of initially polar (red and blue) and initially aligned (black) sister kinetochore pairs over time from acute addition of 3 µM Aurora B inhibitor ZM447439 in CENP-E inhibited (C) and depleted (D) cells, as indicated. (E) Distance to the nearest spindle pole of initially polar kinetochore pairs (blue) over time from acute addition of 3 µM Aurora B inhibitor ZM447439 in CENP-E depleted cells. (F-J) Representative examples of RPE1 cells expressing CENP-A-GFP and centrin1-GFP in different frames following: acute Aurora B inhibition by 3 µM ZM447439 in cells depleted of CENP-E (F), acute Aurora B inhibition by 3 µM ZM447439 in cells pretreated with CENP-E inhibitor with (G, top) and without (G, bottom) addition of the 20 µM proteasome inhibitor MG132, acute Aurora B inhibition by 2 µM ZM447439 and MG132 in cells pretreated with CENP-E inhibitor (H), acute Aurora B inhibition by 120 nM Barasertib and DMSO in cells pretreated with CENP-E inhibitor (I), and acute Aurora B inhibition by 3 µM ZM447439 and DMSO in cells depleted for 48h of WAPL and treated with CENP-E inhibitor (J). Images are maximum projections color-coded by depth as specified by the color bar in Figure 1A. Centrioles are rounded by the white circles. (K) Distance to the nearest centrosome of initially polar kinetochore pairs over time from the treatments indicated at the top of each graph. (L) Distance to the equatorial plane of initially polar kinetochore pairs (top), interkinetochore (inter-KC) distance (middle), and angle between sister kinetochores and the main spindle axis as depicted in the scheme at the top (bottom) over time until alignment of kinetochore pairs in cells where both Aurora B by 3 µM ZM447439 and protein phosphatases by 1 µM Okadaic acid were acutely inhibited in the CENP-E inhibited cells. (M) Distance to the nearest centrosome of initially polar kinetochore pairs over time from respective treatments indicated at the top of each graph. (N) Representative example of an RPE1 cell expressing CENP-A-GFP and centrin1-GFP in different frames as depicted after acute addition of 100 µM Eg5 inhibitor Monastrol in the CENP-E inhibited cell. Time represents the time from the acute treatment. Numbers not given elsewhere: 48 kinetochore pairs from 20 cells in M for CENP-E inhibition and Aurora B inhibition, numbers for other categories are given in the legend of Figure 1E. Statistics: Tukey's HSD test. Symbols indicate: n.s. $P > 0.05$. KC, kinetochore; depl., depletion; inh., inhibitited; react., reactivated; tr, treatment; im, imaging; Con., control; AurB, Aurora B; ABi, Aurora B inhibition.

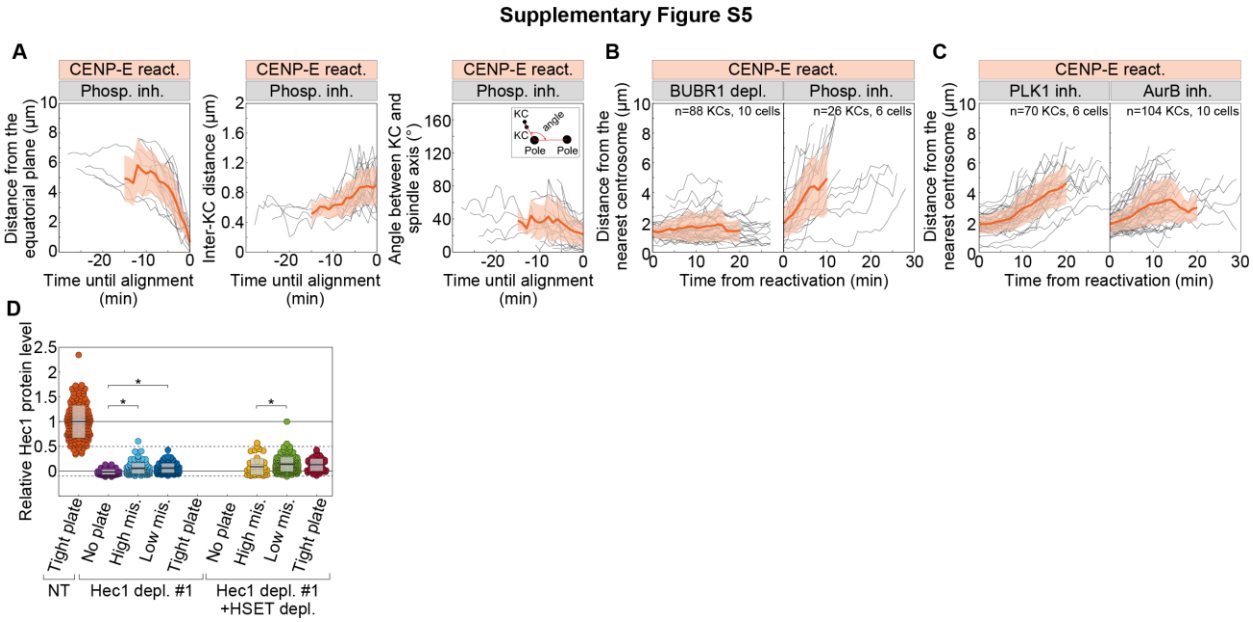

Figure S5. Chromosome congression following CENP-E reactivation does not depend on the activity of protein phosphatases, related to Figure 6. (A) Distance to the equatorial plane of the initially polar kinetochore pairs (left), distance between sister kinetochores (middle), and the angle between sister kinetochores and the main spindle axis, as depicted in the scheme at the top (right), over time until alignment of the kinetochore pair in cells in which protein phosphatases were acutely inhibited by 1 µM Okadaic acid treatment after washout of the CENP-E inhibitor. Thick lines represent means, and grey areas around the means represent standard deviations. (B-C) Distance to the nearest centrosome of initially polar kinetochore pairs over time from the treatment indicated at the top of each graph. (D) Average level of Hec1 on kinetochores normalized to the average of the non-targeting group over treatments and different alignment categories together as indicated at the bottom. Statistics: Tukey's HSD test. Symbols indicate: *$P \leq 0.05$, **$P \leq 0.01$, ****$P \leq 0.0001$. KC, kinetochore; inh., inhibited; depl., depleted; AurB, Aurora B; wash., washout; mis., misalignment.

VIDEO LEGENDS

Video 1. Lattice-light sheet microscopy (LLSM)-based assay for large-scale live cell imaging. Dozens of RPE-1 cells stably expressing CENP-A-GFP and Centrin1-GFP (16-colors) in control cells treated with DMSO, imaged by LLSM right after addition of the drug. Kinetochores and centrioles are color-coded for depth from blue to red with the 16 Colors LUT.

Video 2. RPE1 cells stably expressing CENP-A-GFP and Centrin1-GFP in control and CENP-E reactivated conditions, imaged by LLSM. RPE-1 cells stably expressing CENP-A-GFP and Centrin1-GFP (16-colors LUT) in cells treated with DMSO (control, left) and after wash-out of the CENP-E inhibitor (CENP-E reactivated, right). Cells were imaged right after the addition of the drug (left) or right after drug wash-out (right). Kinetochores and centrioles are color-coded for depth from blue to red with the 16 Colors LUT.

Video 3. RPE1 cells stably expressing CENP-A-GFP and Centrin1-GFP in CENP-E depleted and CENP-E inhibited conditions, imaged by LLSM. RPE-1 cells stably expressing CENP-A-GFP and Centrin1-GFP (16-colors LUT) in cells treated with CENP-E siRNA for 48h (CENP-E depleted, left), and with CENP-E inhibitor (CENP-E inhibited, right). Cells were imaged 48h after addition of CENP-E siRNA (left) or 3h after the addition of the CENP-E inhibitor (right). Kinetochores and centrioles are color-coded for depth from blue to red with the 16 Colors LUT.

Video 4. RPE1 cells stably expressing CENP-A-mCerulean and Mad2-mRuby following reactivation of CENP-E activity, imaged by confocal microscopy. RPE-1 cell stably expressing CENP-A-mCerulean (grey) and Mad2-mRuby (red) in cells treated with CENP-E inhibitor for 3h followed by drug wash-out. Cells were imaged right after wash-out of the drug. Scale bar, 5 μm.

Video 5. RPE1 cells stably expressing CENP-A-GFP and Centrin1-GFP in CENP-E inhibited condition following addition of inhibitors of Aurora kinases, and in CENP-E reactivated condition following depletion of BubR1 and addition of inhibitor of phosphatases, imaged by confocal microscopy. RPE-1 cells stably expressing CENP-A-GFP and Centrin1-GFP (16-colors LUT) in cells treated with CENP-E inhibitor for 3h followed by acute inhibition of Aurora B kinase (top left), acute inhibition of Aurora A kinase (top right), and in cells treated with CENP-E inhibitor for 3h followed by wash-out of the drug in cells depleted for BubR1 (bottom left), and cells acutely treated by phosphatases inhibitor (bottom right). Cells were imaged right after addition of the last drug or drug wash-out. Kinetochores and centrioles are color-coded for depth from blue to red with the 16 Colors LUT and noise was processed with the Despeckle function in ImageJ.